Detection and reconstruction of rock glaciers kinematics over 24 years (2000-2024) from Landsat imagery

Diego Cusicanqui[1], Pascal Lacroix[1], Xavier Bodin[2], Benjamin Aubrey Robson[3], Andreas Kääb[4] and Shelley MacDonell[5,6]

[1]Institut des Sciences de la Terre (ISTerre) CNES, CNRS, IRD, Univ. Grenoble Alpes, Grenoble, 38000, France
[2]Laboratoire EDYTEM, Univ. Savoie Mont-Blanc, Le Bourget du Lac, 73376, France
[3]Department of Earth Science, University of Bergen, Bergen, Norway
[4]Department of Geosciences, University of Oslo, Oslo, 0316, Norway
[5]Centro de Estudios Avanzados en Zonas Áridas (CEAZA), La Serena, Chile
[6]Waterways Centre, University of Canterbury and Lincoln University, Christchurch, New Zealand

Correspondence to: Diego Cusicanqui (diego.cusicanqui@univ-grenoble-alpes.fr)

Abstract. Rock glacier velocity is now widely acknowledged as an Essential Climatic Variable for permafrost. However, representing decadal regional spatiotemporal velocity patterns remains challenging due to the limited ~~number~~availability of high-resolution (<5 m) remote sensing data. In contrast, m~~M~~edium resolution satellite data (10-15 m) is ~~on the contrary~~ globally available over several decades~~, and~~ but has ~~never~~not been used for rock glacier kinematics. This study presents a robust methodological approach ~~based on the~~combining pairwise feature tracking image correlation ~~using~~with medium-resolution Landsat 7/8 optical imagery~~, together with the inversion of~~ surface displacement time-series inversion, and the automatic detection of persistent moving areas (PMA). ~~a~~Applied to rock glacier monitoring in the Semi-Arid Andes of South America~~.~~ t~~T~~his methodology enables the detection and quantification of surface kinematics of 153 rock glaciers, 124 landslides and 105~~229~~ ~~382~~ unclassified~~gravitational slope mass movements (153 corresponding to rock glaciers)~~ over ~~a~~ 24-years~~, over an area of~~across a 2250 km² area. This is the first time that Landsat images have been used to quantify rock glacier displacement~~s~~ time-series~~and derive velocities~~. ~~From this we derive~~The study estimates an average velocity of 0.37 ± 0.07 ~~m a~~m yr^{-1} over 24 years for all rock glaciers, with some ~~exceptions where~~ large rock glaciers and debris frozen landforms exhibiting surface velocities exceeding 2 ~~m a~~m yr^{-1}. The results ~~of this study show a good agreement~~align well with results from high-resolution imagery~~, and~~ recent ~~in-situ~~GNSS measurements, and previous inventories. However the L7/8 imagery-derived velocities are ~~on average~~ underestimated by approximately 20-30%~~.~~ on average. Additionally, ~~the relatively~~ high uncertainties between consecutive image pairs make it challenging to interpret annual velocity variations. Nevertheless, decadal velocity changes were observed in ~~3~~2% of PMAs, where ~~threesix~~two (one) rock glaciers show~~ing~~ a significant~~11%~~ acceleration (deceleration) ~~increase and six rock glaciers showing an 18~~41% ~~of significant deceleration decrease in velocity~~ over two~~one~~ decades. Our calculations show that decadal velocity changes < 0.4 m yr^{-1} are associated with high uncertainty when using L7/8 data, with sensitivity depending on the reference period. ~~Our study suggestsalso~~Our

results highlights some relations between topographic parameters as ~~a control of velocity mostly based on~~ the PMA~~rock glacier~~ size, ~~as well as~~ the orientation, slope and elevation, ~~controls the position of the active zones,~~ suggesting that permafrost thaw influences the ~~location~~ occurrence of high-altitude landslides ~~in the Andes~~. This study demonstrates the feasibility of using medium-resolution optical satellite imagery for monitoring rock glacier velocity~~s~~ ~~globally~~ over several decades.

1 Introduction

Historically, the state of the cryosphere has been ~~measured~~ assessed using specific variables defined by Global Climate Observing System ~~(GCOS)~~ (GCOS, 1995), ~~such as~~including mass balance for glaciers, snow cover variability ~~for snow~~ and ground temperature for permafrost. Among those variables, glacier mass balance and snow cover variations are relatively well known at a global scale (Hugonnet et al., 2021; Notarnicola, 2020) compared to changes in mountain permafrost, which is~~are~~ still very incompletely monitored (Bolch et al., 20~~20~~19).

Permafrost is an important component of the cryosphere occurring at high latitudes (i.e. polar regions) and high elevations (i.e. mountainous areas). As permafrost —ground material remaining at or below 0°C for at least two consecutive years— is a thermal phenomenon, it is thus sensitive to changes in climate forcing (Hock et al., 2019). ~~The evidence of m~~Worldwide estimation of m~~M~~ountain permafrost warming relies on very few direct borehole observations (Noetzli et al., 2019), distributed mostly in the western Alps and Alaska, leaving ~~. Thus, several~~ many mountain ~~ranges~~ regions without adequate ~~are lacking sufficient permafrost~~ monitoring data ~~to analyse changes~~. Mountain permafrost degradation ~~is indicated~~ manifests by the increase in ground temperatures and active layer thickness (Etzelmüller et al., 2020), the increase of liquid water content within the frozen terrain (Cicoira et al., 2019), as well as ground-ice melt (Cusicanqui et al., 2021; Haberkorn et al., 2021). These changes also favour~~intensify~~ landslides~~mass movements, (~~the downslope movement of soil, rock, and organic materials under the force of gravity~~), often influenced by water, seismic activity, or human activities~~; ~~(USGS, 2004)~~. For instance, recent~~More recently,~~ warming~~-induced ground destabilization can~~ induces~~lead~~ an increased frequency of ~~to~~ landslides~~, defined as the gravitational movement of rock, debris, or earth down a slope due to gravity~~ (Pei et al., ~~USGS,~~ 202~~0~~34). However, warming affects mountain permafrost differently according to the type of terrain, ~~reflecting in~~ particularly due to ~~particular the influence of~~ the snow cover influence~~on the ground~~. ~~While a rather steady warming trend can be observed in steep rock slopes~~ Steep rock slopes, where snow is scarce, exhibit a steady warming trend (Magnin et al., 2024), where~~as snow is poorly present, permafrost temperatures in~~ loose rock formations such as rock glaciers show pronounced inter-annual variations, mostly due to the variable insulating effect of snow (Thibert & Bodin, 2022; Kellerer-Pirklbauer et al., 2024).

In the present paper, we follow the definitions proposed by the IPA Rock Glaciers Inventory and Kinematics (RGIK) action group, stating that rock glaciers can be defined as "debris landforms generated by the former or current creep of frozen ground (permafrost), detectable in the landscape with the following morphologies: front, lateral margins and optionally ridge-and-furrow surface topography" (Berthling, 2011; RGIK, 2023). Given the complexity of measuring permafrost warming, rock glacier velocity has been recently proposed and accepted by the GCOS to be a complement of the Essential Climatic Variable (ECV) -permafrost (Hu et al., 2023). ~~Indeed, t~~The thermally-dependent creep of ice-rich frozen ground is inherently sensitive to climatic conditions and ~~it is able to change~~ fluctuates over different timescales (Delaloye et al., 2010; Kääb et al., 2007; Sorg et al., 2015). ~~While the variation of creep velocities at i~~Inter-annual, seasonal and ~~over~~ short-term ~~time-scales reflects mainly the influence of weather~~variations in creep velocity primarily reflect weather influences (Kenner et al., 2017; Wirz et al., 2016), while long-term ~~patterns~~ trends — decadal to pluri-decadal ~~scales~~— correlate ~~relate primarily to~~ with mean annual air or ground temperatures (Pellet et al., 2022, Kellerer-Pirklbauer et al., 2024).

Since the early 2000s, there ~~has been~~is a growing interest from the international community in ~~the~~ monitoring ~~of~~ rock glacier velocities~~y~~. ~~Indeed, o~~Observations ~~show~~ indicate that rock glacier velocities often exhibit similar interannual to long~~er~~-term trends at a regional scale (Kellerer-Pirklbauer & Kaufmann, 2021; Marcer et al., 2021; Pellet et al., 2022), ~~which strongly depends on~~ largely driven by local ground temperature changes (Noetzli et al., 2019). ~~The v~~Velocity of rock glaciers is controlled by the landform's intrinsic characteristics ~~of the landform~~, ~~in~~ particularly its internal structure (ice / debris proportions, thickness) and the topography (bed slope ~~of the bed~~), while external climatic factors—such as ground temperature, advection, infiltration, and internal meltwater production—also play a significant role~~but it is also influenced substantially by a external climatically-driven factors such as ground temperature and advection, infiltration, or internal meltwater production and routing~~ (Jansen and Hergarten, 2006; Cicoira et al., 2019a; Kenner et al., 2020). Thus, the magnitude and variability of their velocity can give an indication on~~as to~~ their current state and possible ongoing changes in the characteristics of the permafrost body. ~~The m~~As a consequence, m~~M~~onitoring ~~of changes in~~ rock glacier velocity changes ~~thus~~ provides information about the impact of climate change on mountain permafrost ~~kinematics and~~, indirectly, on its thermal state. Given the observed current warming context of mountain permafrost (Noetzli et al., 2019), the velocity~~creep speed~~ of rock glaciers in cold mountains is expected to increase with ground temperature (Arenson et al., 2015; Kääb et al., 2007; Müller et al., 2016).

Quantifying rock glacier velocity ~~over~~ at regional scales has been first~~most~~ ~~successfully~~ ~~effectively~~ achieved using satellite radar interferometry (InSAR) data. This method enables the detection of slow slope movement (i.e. rock glacier motion) in the satellite's Line of Sight (LOS) ~~of the satellite, over~~across large regions and hundreds of individual landforms (Hu et al., 2023). This approach has been used to map rock glacier motion around the world (Bertone et al., 2022). This data source has served as a base for classifying movement~~s~~ rates of various orders of magnitude (cm/d, cm/month, dm/month, cm/a, etc.), recently standardised within the RGIK group (RGIK, 2023). However, even if this technique is well suited for rock glacier

mapping (Barboux et al., 2014), it is ~~satellite radar interferometry is~~ most effectivesuitable for relatively slow rock glacier speeds, with maximum detectable speed~~s~~ of approximately 1–1.5 ~~m a~~m yr^{-1} ~~observed~~ over short observation periods (6, 12 days). Beyond this threshold, InSAR signals become geometrically decorrelated and thus uninterpretable (Villarroel et al., 2018). In addition, freely available high-temporal-resolution SAR data ~~with high temporal resolution~~ has only been ~~available~~accessible since the early 21st-century (Strozzi et al., 2020), preventing the assessment of . ~~This means that no~~ climatic timescales (i.e. ~~decennial timescales~~decadal trends) for rock glaciers ~~can be obtained with this source of data~~velocity.

Comparatively, optical imagery offers a more robust alternative ~~where~~ applying feature ~~-~~tracking techniques ~~can be applied~~ to repeat and historical imagery to derive rock glacier surface displacements and velocity, ~~both to contemporary imagery and historical datasets, allowing rock glacier velocities to be investigated~~ over extended~~longer~~ timescales (Cusicanqui et al., 2021; Kääb et al., 2021; Kaufmann et al., 2021). This technique is ~~not well~~less suitable for slow velocities due to ~~its~~a low signal-to-noise ratio (unless very high spatial resolution allows tracking the movement), but ~~rather~~ is well suited for medium to large movements beyond 1 - 1.5 ~~m a~~m yr^{-1} (Hartl, et al., 2021; Marcer et al., 2021). T~~However, t~~o date, applications ~~such techniques~~ have been ~~exemplified~~ limited ~~on rock glaciers using~~to high resolution optical imagery (<5 m), often requiring ~~. Very often, using~~ airborne imagery that is ~~not easily accessible, can be~~ prohibitively expensive for larger regions or for more extensive time series. As a consequence, few periglacial ~~areas~~ regions have been extensively investigated using feature tracking, with ~~a~~most ~~of the~~ research focus~~ed~~ ~~studies restricted to~~ on the European Alps (Cusicanqui et al., 2021; Hartl et al., 2016; Kellerer-Pirklbauer and Kaufmann, 2012), some isolated regions in the Andes ~~i.e. Tapado rock glacier~~ (Vivero et al., 2021; Blöthe et al., 2021), in northern Tien Shan (Kääb et al., 2021; Wood et al., 2025) and more recently, ~~in~~ the United States (Kääb and Røste, 2024).

Medium~~-~~-resolution imagery (Landsat-4/5/7/8, SPOT 1-4, ASTER) has ~~offered a~~provided continuous data~~set~~ for monitoring slow-moving landforms since the 1980's. Recent progress in time-series processing has~~has~~ve enabled the development of methods for both detecting and monitoring slow-moving landslides using medium-resolution imagery over the last 40-50 years (Bontemps et al., 2018; Lacroix et al., 2020a). However, t~~T~~hese methods have never been ~~used~~ applied to~~for~~ rock glaciers due to their ~~because of (1) the rather~~ slow motions ~~of rock glaciers overall~~ (~ 1 ~~m a~~m yr^{-1})~~,~~ and ~~(2)~~ the ~~difficulty~~ challenges posed ~~of the processing caused~~ by the presence of snow and shadows in steep mountains ~~topography~~. Here, we demonstrate the applicability of the free and open-access, global, medium-resolution satellite datasets Landsat 7/8 (called hereafter L7/8) to characterise rock glacier displacements and velocities~~y~~ for the early 21th century in a region of the semiarid Andes (both on Chile and Argentina). We further validate our results at a regional scale using Sentinel-1 wrapped interferograms, and at a ~~more~~ local scale with very high resolution (called hereafter VHR) datasets e.g. Geoeye, Pléiades, airborne on the Tapado complex area and recent Global N~~n~~avigation S~~s~~atellite S~~s~~ystem (GNSS) measurements.

2 Study area and previous work

Our study area ~~is located~~ lies within the Coquimbo and San Juan provinces, in the semiarid Andes of Chile and Argentina (~~between~~ 29°20'S ~~and~~ -31°15'S ~~latitude~~; Fig. 1). It ~~is a~~covers ~45x45 km² ~~site~~, with altitudes ranging ~~between~~from 3,000 ~~and~~to 6,300 m above sea level (a.s.l). The regional climate is characterised by semi-arid conditions, influenced mainly ~~influenced~~ by the subtropical South Pacific anticyclone (Montecinos & Aceituno, 2003). The rugged topography from coastal locations~~position~~ to the high-elevation of the Andes mountain range (~6,000 m.a.s.l.) ~~have a strong influence on the general~~ strongly affects atmospheric circulation, ~~notably~~ differentiating the eastern and western climatic ~~systems~~regimes (Kalthoff et al., 2002). Schauwecker (2022) shows that ~~the~~ precipitation ~~coming~~ from ~~the~~ humid Pacific air masses occurs almost exclusively as snowfall~~, and mostly~~ concentrated in the austral winter ~~(, between~~ May ~~and~~ -August~~)~~. Year-to-year precipitation varies notably in accordance with the El Niño Southern Oscillation (ENSO) phenomenon with above (below) -average precipitation during El Niño (La Niña) events (Masiokas et al., 2006, 2010) with recent deficits in precipitations between 20-40% (Garreaud et al., 2020). ~~Recent m~~Meteorological records by~~on~~ three Automatic Weather Stations (AWS) show mean annual precipitation of ~170 mm in the last decade (CEAZA, 2023). Recent ~~studies of the~~ air temperature studies ~~have~~ show~~n~~ a warming trend of 0.2°C per decade in the central Andes, ~~closely~~ contributing to~~influencing the~~ decreasing~~e in~~ snowfall~~s~~ (Poblete & Minetti, 2017; Réveillet et al., 2020).

According to global permafrost distribution models (Gruber, 2012; Obu, 2021) and a local one (Azócar et al., 2017), heterogeneous/discontinuous permafrost ~~is present~~occurs between 3,900 - 4,500 m a.s.l., becoming ~~more prevalent~~ widespread above 4,500 m a.s.l. (Fig. 1). ~~In this context, s~~Several rock glacier inventories ~~have been carried out along~~ exists for the Chilean (DGA, 2022) and Argentinian (IANIGLA, 2018) Andes~~,~~ a~~s well as several~~longside detailed/local geomorphological investigations (Monnier & Kinnard, 2015, 2016, Halla et al., 2021; Navarro et al., 2023; de Pasquale et al., 2022). According to both inventories of Chile and Argentina ~~(, both of which are~~ both based on geomorphological interpretation of optical satellite imagery~~),~~ the area has a relatively high number of rock glaciers with 80 located on the Chilean side and 235 on the Argentinian side (Fig. 1). The study of mountain permafrost in this ~~particular~~ region of the semi-arid Andes has received attention during the last decades because of the high density and large extension of rock glaciers (Janke et al., 2015). ~~Most r~~Recent studies highlight the complex interaction between remnants of glaciers, debris covered glaciers and rock glaciers (Navarro et al., 2023a; Robson et al., 2021) as well as the ~~importance~~role of rock glaciers as water storage resources (MacDonell et al., 2022; Schaffer et al., 2019; Schaffer and MacDonell, 2022).

Despite ~~this~~growing interest, ~~a~~ limited information is available~~overview of the status~~ o~~n~~f rock glacier velocities ~~exist~~, and~~while~~ historical velocity trends ~~of velocity largely remain unknown~~. ~~For instance,~~ Villarroel et al. (2018) provided a ~~recent~~ kinematic inventory of the Argentinean Andes ~~(, between~~ 30.5°S- and ~~-~~33.5°S~~)~~, identifying ~2100 active rock glaciers ~~based on~~using InSAR. On the other hand, Blöthe et al (2021) provided a regional assessment in the "Cordon del Plata" range

(~300 km south of our study area), quantifying velocity fields of 244 rock glaciers between 2010 and 2017/18 using offset tracking between optical imagery. Only two rock glaciers ~~monitoring~~ in this region are monitored i.e. Dos Lenguas rock glacier studied ~~mostly~~primarly with InSAR (Strozzi et al., 2020) and more recently with Uncrewed Aerial Vehicle (UAV; Stammler et al., 2024) in Argentina and the Tapado complex in Chile (Vivero et al., 2021), monitored ~~with GNSS data~~ since 2009 ~~and with~~using GNSS and historical aerial images, ~~being the only~~ providing the longest surface velocity time series since the 1950's. In this sense, a historical perspective ~~is still lacking in the region~~on velocity trends remains largely absent in this region. Finally, this region was chosen due to good coverage of reference datasets, namely VHR satellite imagery and in situ GNSS measurements on the Tapado rock glacier (DGA, 2010), which serve as ~~that could be used for~~ validation sources.

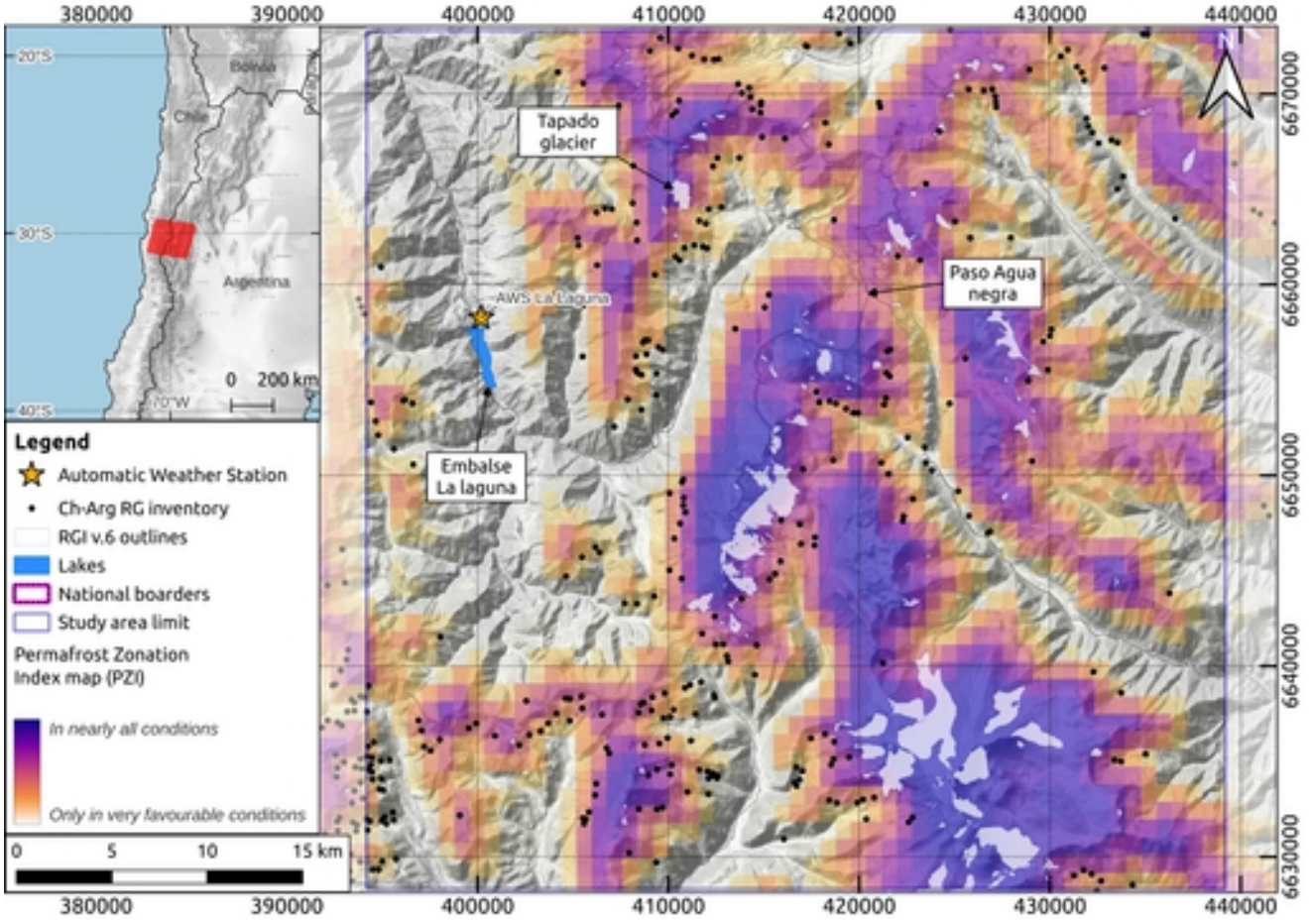

Figure 1: Location of the study area in the semiarid Andes (~~between~~ 29°20'S ~~and~~ -31°15'S ~~latitude~~). ~~R~~The red square in the inner map shows the footprint of the Landsat scenes used in this study. Within the main map, black dots correspond to rock glacier inventory for Chile (DGA, 2022) and Argentina (IANIGLA, 2018). The orange-purple colorbar represents the Permafrost Favorability Index (PFI) from (Gruber, 2012). A comparison with the more recent PFI from Obu (2021) is shown in Fig. S1. Background map corresponds to © OpenTopoMap.

3 Data

Three different remote sensing datasets were used in this study: (1) L7/8 images, (2) VHR images from airborne platforms and satellites, used to validate the L7/8 products temporally, and (3) Sentinel-1 SAR interferograms, used to validate the L7/8 products spatially. Additionally,~~We also used~~ GNSS data ~~acquired on~~from a ~~one~~ specific rock glacier was~~wer~~ used for ~~the~~ kinematic validation.

3.1 L7/8 dataset

The L7/8 dataset comprises freely ~~and open~~ available 8-band multispectral orthorectified satellite images spanning ~~the period from~~ 2000~~- to~~ 2024 period (Fig. 2a and b). ~~We used o~~Only the ~~L7/8~~ panchromatic band (B8) was used, with the highest spatial resolution (15 m). ~~However, d~~Due to the Scan Line Corrector failure on the Landsat-7 satellite ~~(between~~ 2004 ~~and~~ 2013~~; (~~Markham et al., 2004), ~~we excluded Landsat-7~~ scenes from~~within~~ this period were excluded to avoid data gaps. All images correspond to path~~/ and~~ row 233/081~~, and have been~~They were cropped to~~within~~ a common grid (3001x3001 pixels) ~~corresponding to a surface area~~covering ~~of~~ 45x45 km². One image per year was ~~chosen~~ visually selected during the summer months (January to ~~-~~April)~~,~~ to avoid~~minimize with the goal of obtaining the least~~ snow and cloud cover ~~possible~~ (Table S1).

3.2 VHR dataset

The VHR dataset comprises high-resolution satellite orthoimages acquired at irregular intervals between 2000 and 2020 (Fig. 2b). These images comprise ~~a combination of~~ data from three different sensors~~:~~, ~~namely~~ aerial (0.5 m), Geoeye (0.5 m) and Pleiades (0.7~~5~~ m). In this dataset, the panchromatic image ~~s~~bands ~~have been~~were orthorectified and resampled within the same grid with a spatial resolution of 1x1 m. Given the variable spatial coverage of the VHR datasets, ~~we have selected~~ two sub-areas (i.e. Tapado and Largo RG sub-regions, respectively; Fig. 2) were selected ~~where the largest amount of imagery is available attempting~~ to ~~maintain~~assure a temporal coverage comparable to th~~cat of the~~ L7/8 dataset.

~~With regard to the processing~~Most of the VHR ~~dataset~~images~~, the majority of the images~~ were already orthorectified and used directly by~~from~~ Robson et al., (2022), except for: *(i)* the photogrammetric flight in 2000's and *(ii)* the 2014 Pleiades acquisition. Regarding the 2000's photogrammetric flight, ~~we undertook a re-processing of the~~ data were reprocessed to ~~by~~ extend~~ing~~ coverage ~~the area~~ to the Largo rock glacier (4 km north from Tapado complex area; Fig. 2d) ~~which was not~~ initially ~~covered~~omitted in Robson et al., (2022). The photogrammetric processing was based on the method set out by Cusicanqui et al., (2021) using Agisoft Metashape software v. 2.0.3 (Smith, 2011). Sixteen Ground Control Points (GCPs) were used a~~round~~cross both ~~small~~ sub-areas, with~~:~~ t~~T~~he 2019 Pleiades DEM ~~has been employed~~serving as a reference for the GCPs (Robson et al., 2022). A coregistration st~~epage~~, based on ~~using~~ Nuth & Kääb (2011), ~~methodology was undertaken to~~ correct~~ed~~ small shifts ~~of~~in the 2000's aerial DEM.

~~With regard to~~For the 2014 Pléiades ~~2014~~ acquisition, processing followed ~~we applied the same methodology described in~~ Cusicanqui et al., (2023) to process the ~~Pléiades 2014~~ stereo pair without GCP's~~, and~~ using only Rational Polynomial Coefficients (RPC). The 2014 stereo DEM was subsequently coregistered ~~afterwards to~~ the 2019 Pléiades DEM~~, and~~ ~~Subsequently, the~~ orthoimages were adjusted ~~in~~ accordingly~~ance with the aforementioned DEM co-registration values~~. Finally, VHR images were acquired during the dry season ~~(between~~ November~~-~~ to April~~),~~ ~~spanning~~over almost two decades (Table S1).

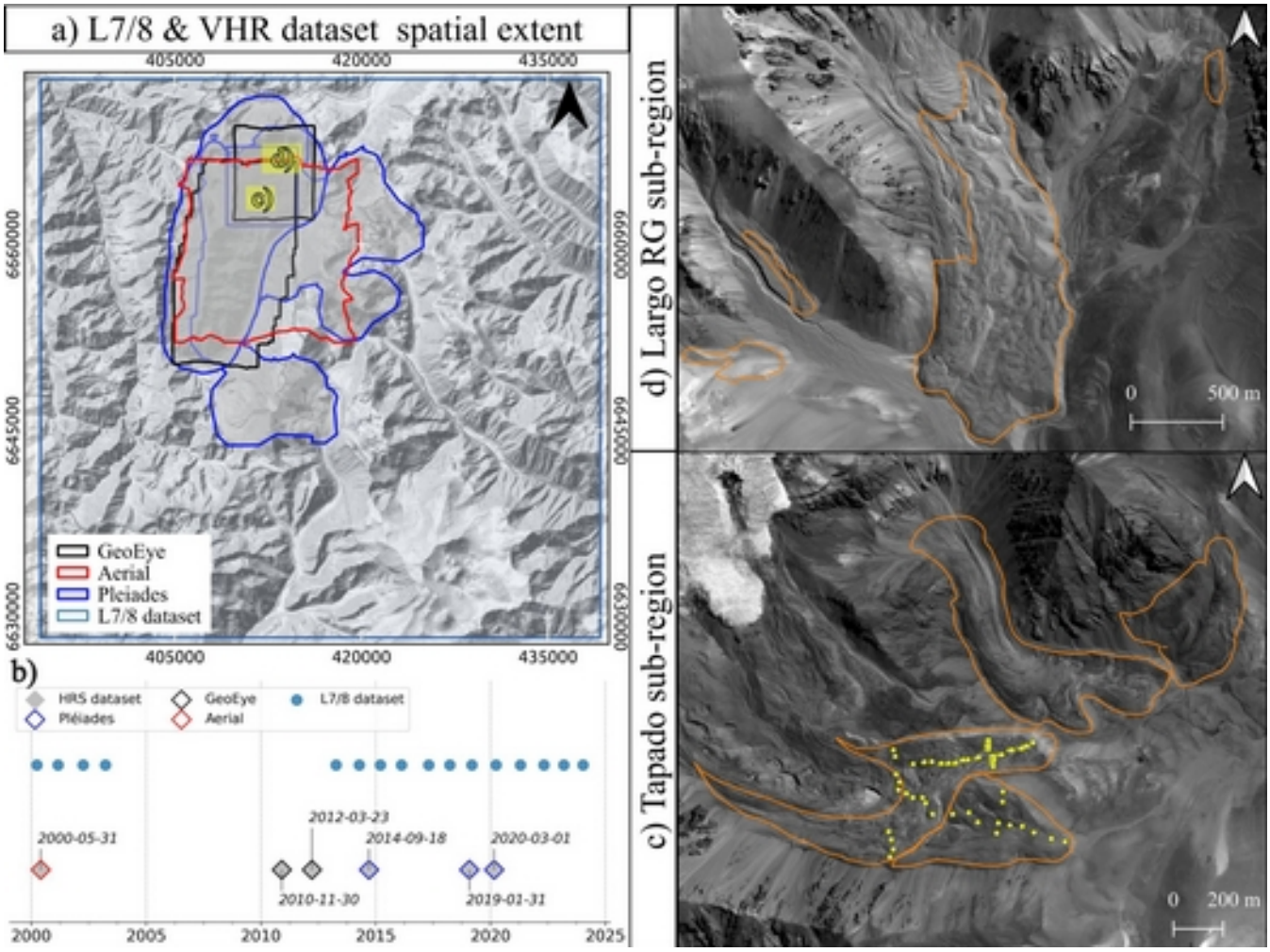

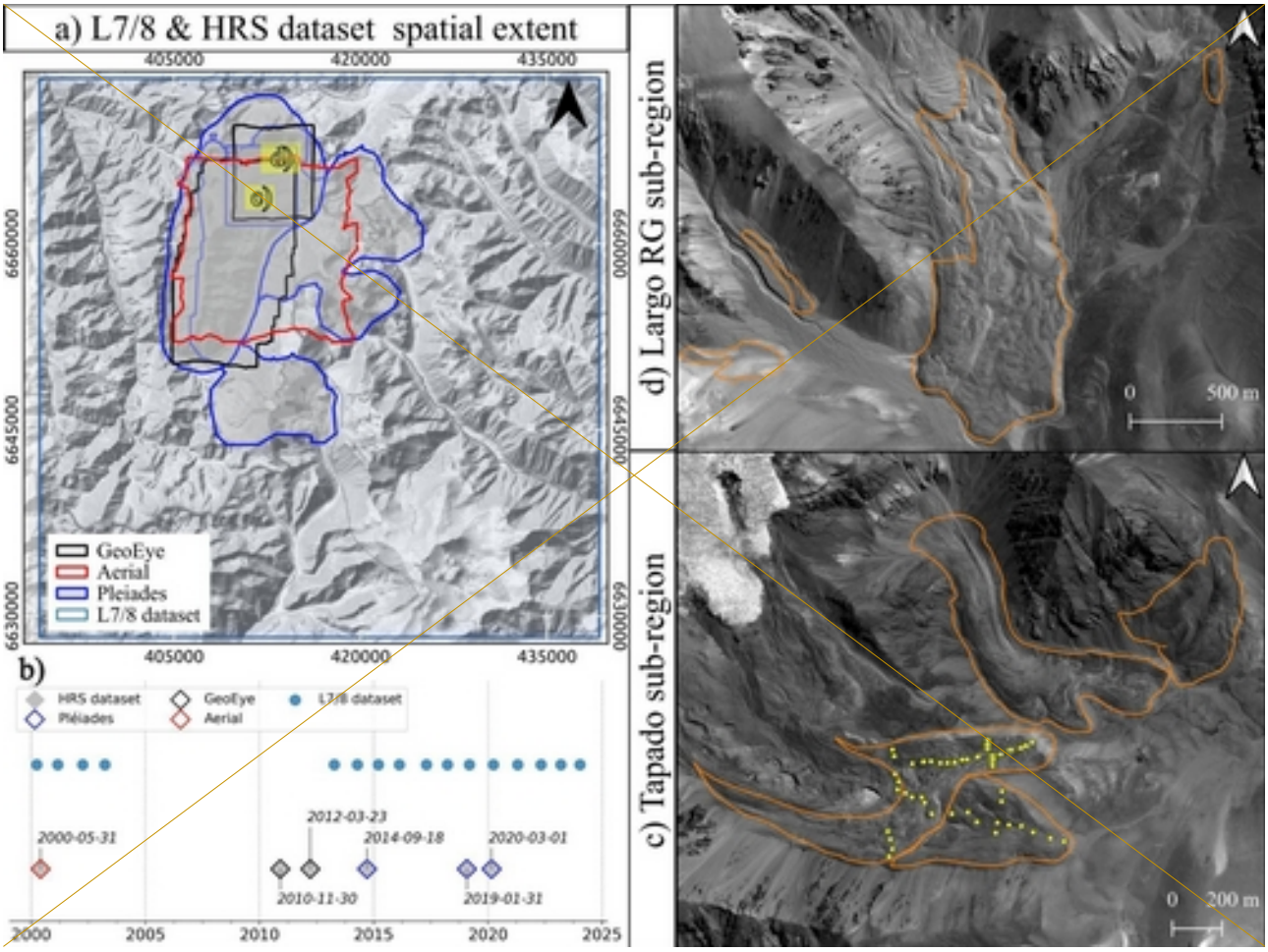

Figure 2: a) and b) Spatial extent and temporal distribution of L7/8 and VHR datasets, respectively; c) and d) Zoom over high resolution sub-regions used for validation. Orange polygons represent the 2013 rock glacier inventory from DGA, (2010) and yellow-dots represent the GNSS network on the Tapado complex (CEAZA, 2023). Image backgrounds correspond to © OpenTopoMap for a) and Pléiades 2019 imagery © CNES/AIRBUS for c) and d).

3.3 Sentinel-1 interferograms

Due to the limited spatial extent of the VHR dataset, we used raw Sentinel-1 wrapped interferograms to validate the classification of the L7/8 surface displacement products ~~(cf. Section 4.1) as well asnd tfor classifying rock glaciers and the inventory of gravitational mass movements including rock glaciers and landslides~~ (cf. Section 4.3). This analysis ~~was conducted through a~~involved visual inspection~~inspecting~~ of~~on of several~~multiple interferograms covering the entire study area. Sentinel-1 interferograms were processed using the ForM@Ter LArge-scale multi-Temporal Sentinel-1 InterferoMetry processing chain —FLATSIM— service (Thollard et al., 2021) at different temporal baselines (~~i.e.~~ 12, 60 and 360 days). ~~For~~

tThis study, we employed utilized 40 interferograms from early winter 2022 untilto late winter 2023 in both ascending and descending orbits (paths 120 and 156, respectively; Table S2). These interferograms were averaged in 2-looks (2 pixels in azimuth, 8 pixels in range) in radar geometry, equivalent to about 30 metres in terrain geometry. In brief, the FLATSIM service systematically produces interferograms from Sentinel-1 data and displacement time series, over large geographical areas. This service is based on the InSAR "New Small temporal and spatial BASelines" (NSBAS) processing chain as described in Doin et al., (2011) and Grandin (2015). FLATSIM products were corrected topographically using a SRTM-DEM and atmospherically corrected using ERA-5 atmospheric model mapped on the DEM. Full details can be found in Thollard et al., (2021) and ForM@TER platform.

3.4 GNSS data

The surface kinematics of the Tapado rock glacier have been measured since 2009 over 61 points (DGA, 2010) by the Centro de Estudios Avanzados en Zonas Áridas (CEAZA), using a differential GNSS (dGNSS) sonsisting . This network consists of a survey of 61 points measured since 2009 using a differential GNSS (dGNSS) system (DGA, 2010). According to CEAZA (2012, 2016) and Vivero et al. (2021), the base station coordinates were fixed using the Trimble CenterPoint RTX post processing service, and the while differential post processing of the GNSS raw data between this base and the rover GNSS antenna wcreas processed conducted with using Trimble Business Center software (TBC, V.4) surveying software. The reported average horizontal and vertical precisions (95%) were 0.02 and 0.04 m, respectively. In order tTo address some inconsistencies oin point locations i.e. points systematically shifted by few metres in north-east direction, 14 groups of GNSS points corresponding to the same block and specific dates (i.e. 2013-12-11, 2022-04-06, 2010-12-06) were removed from the original dataset. The remaining dataset comprises 47 groups of points and has been employed was primarily used tofor the validatcion of surface velocity maps derived from both L7/8 and VHR dataset (cf. Section 5.3). Additionally, as no GCPs exist for Largo rock glacier, we manually tracked 13 pseudo-GCPs were manually tracked on representative features clearly identified on the VHR dataset to compare with L7/8 dataset (cf. Section 5.3).

4 Methods

OurThe methodology employed in this study is based relies on the feature-tracking offset image correlation strategy, which involves the analyzingsis of a large number of images available for athe site. Subsequently, inversion of time-series techniques were applied to the correlated images in order to derive consistent surface displacement fields over time (Section 4.1). Then, a medium-resolution DEM was used to identify Persistent Moving Areas (PMAs) along the slope direction within the study region (Section 4.2). EventuaFinally, we validate the final surface velocity fields by comparing them to recent dGNSS measurements and feature tracking of both L7/8 & VHR datasets oin two small sub-regions in the upper regions of the La Laguna catchment (i.e. Tapado region).

4.1 Inversion of displacement time-series

Horizontal displacement time series were derived from L7/8 and VHR orthorectified images, following a similar approach developed in Bontemps et al., (2018), classicallypreviously applied on slow moving landslides (e.g. Lacroix et al., 2019). The method used in in this study is summarized as follows:

a) Feature tracking image correlation was performed in all possible pairwise combinations and their permutations (i.e. forward and backward). Two different software were used for each dataset. Firstly, we used Mic-Mac (Rupnik et al., 2017) through the Normalised Cross Correlation (NCC) algorithm to correlate images within the L7/8 dataset. This software was selected for its ability to handle images with low radiometric contrast and for small objects (Lacroix et al., 2020ab). Secondly, the Ames Stereo Pipeline (ASP) (Beyer et al., 2018) was employed to correlate image pairs within the VHR dataset. In ASP, the More Global Matching (MGM) implementation (Facciolo et al., 2015) was used to perform image correlation. The MGM algorithm reduces high-frequency spatial artefacts (compared to classic NCC algorithms) in textureless regions and produces smooth surface displacement fields. Image mismatches associated with georeferencing errors are minimised due to the pre-alignment strategy (i.e. automatic identification of image features matched in a pair of images used then as tie-points) before the feature tracking stage. Both softwares present an adaptive windows matching strategy corresponding to 3x3 for MicMac and 7x7 for ASP as the smallest window size.

b) In both cases, all pixels with low correlation coefficient values (CC < 0.6) and displacement magnitudes > 120 m, were masked. Furthermore, an additional glacier outline masking step was applied to the VHR dataset, to avoid noisy displacement values due to glacier retreat. The Randolph Glacier Inventory (RGI v.6) was used as the source of glacier outlines (RGI Consortium, 2017).

c) Additionally, thea median surface displacement value was subtracted from the total displacement fields on both east-west (EW) and north-south (NS) displacement maps for all pairsdates. The mMedian value was computed over the entire EW and NS products computing each one for their specific dates.

d) For the L7/8 dataset, striping effects from sensor inter-band misalignments (Ayoub et al., 2008; Leprince et al., 2008) were mitigated by subtracting the median value of the stacked profile in the along-stripe direction, considering only stable areas (cf. Section 4.3).

e) A least-squares inversion was applied to the redundant displacement pairs for each pixel, separately for EW and NS components (Bontemps et al., 2018). This process reduced uncertainties by approximately 30%, as shown in prior applications on SPOT 1-4 images. A weight strategy can be added to the different pairs during the inversion, to take into account the surface-cover changes over time. Due to the arid and natural cover of our area of study, this weight is not used here.

4.2 Automatic extraction of PMAs

The ~~time series of~~ cumulative surface displacement~~s~~ time-~~-~~series from L7/8 images ~~are then~~ were used to automatically extract PMAs. ~~The~~ PMA~~s are a group~~consist of connected pixels ~~having a~~ displaying coherent movement ~~in~~over time, and following the downslope direction, as ~~this is~~ expected for ~~motions driven by~~ gravity-driven processes (e.g. rock glaciers, landslides) or ~~other~~ erosional~~sive~~ processes (e.g. shifting rivers, river bank~~s~~ erosion). ~~Briefly, t~~This methodology, developed by Stumpf et al., (2017), proposes to use the direction coherence of the displacement (called the vector coherence) with time to detect active pixels. A TanDEM-X World DEM with 12 m resolution, smoothed with a 7x7 median filter~~windows size~~ (approximately 90 m) was used to compute the slope orientation ~~to detect~~ and identify pixels consistent with gravitational movements. ~~Namely we remove p~~Pixels ~~whose~~ with mean velocity vectors deviating~~ed~~ by more~~are oriented less~~ than 45° from the downslope direction (calculated over a 200m kernel size ~~of 200 m~~) were removed~~-~~ to ~~take into~~ account for~~the relatively~~ large-scale topographic undulations ~~of the topography~~. These ~~relatively~~ higher parameter~~s~~ thresholds ~~have been chosen~~ were selected after ~~a series of~~multiple trials, ~~and take into account~~considering the lower resolution of the images used compared to Stumpf et al., (2017), and the presence of snow in high mountains that can alter the quality of the displacement fields. Following this pixel-based approach, isolated pixels ~~are~~ were removed.

4.3 PMA characterisation using InSAR and high resolution imagery

As mentioned in Section 3.3, InSAR wrapped interferograms were used mainly for validation and characterization of automatic PMA detection. Rather than create a new inventory of moving areas, we manually checked all polygons resulting from PMA methodology (cf. Section 4.2) against the interferograms. ~~As suggested~~Following ~~in~~ Barboux et al.~~,~~ (2014) and RGIK~~,~~ (2023), ~~we used~~ a combination of all available interferograms (Table S2) with high resolution Google Earth imagery was used to classify ~~slope movements~~PMAs. ~~During this analysis, we consider the~~A PMA was considered 'confirmed' if its~~when the~~ polygon overlapped a clear InSAR fringe pattern at any interval (~~e.g.~~ 12, 60 and 360 days~~) on the interferograms~~ (~~,~~ Fig. 3). The final classification consisted of two categories~~analysis resulted in a binary class,~~; 'confirmed' and 'not confirmed'. ~~Secondly~~Additionally, a simple geomorphological class based on high resolution Google Earth imagery was assigned to each polygon. The geomorphological class reflects the landform overlapping the PMA ~~polygon~~. For instance, a landslide class was assigned when cracks and scarps were present at the surface. Rock glacier class was assigned when typical morphology (i.e. front and lateral margins with ridge-and-furrow surface topography) was observed. When no clear interpretation about the movement and the geomorph~~ology~~ic interpretation could be assessed on either InSAR or Google-Earth basemaps, the 'unclassified' class was assigned to those PMA. ~~the PMA was classified within theas 'other' geomorphological class~~. These features ~~are~~ were often ~~located not so far from the~~ near ridges ~~and at the~~or valley bottoms (i.e. river banks erosion, road construction, …). Finally, ~~we also assigned~~ a velocity class ~~for~~to each PMA was assigned~~,~~ based on RGIK (2023) recommendations (cf. Section 6.2).

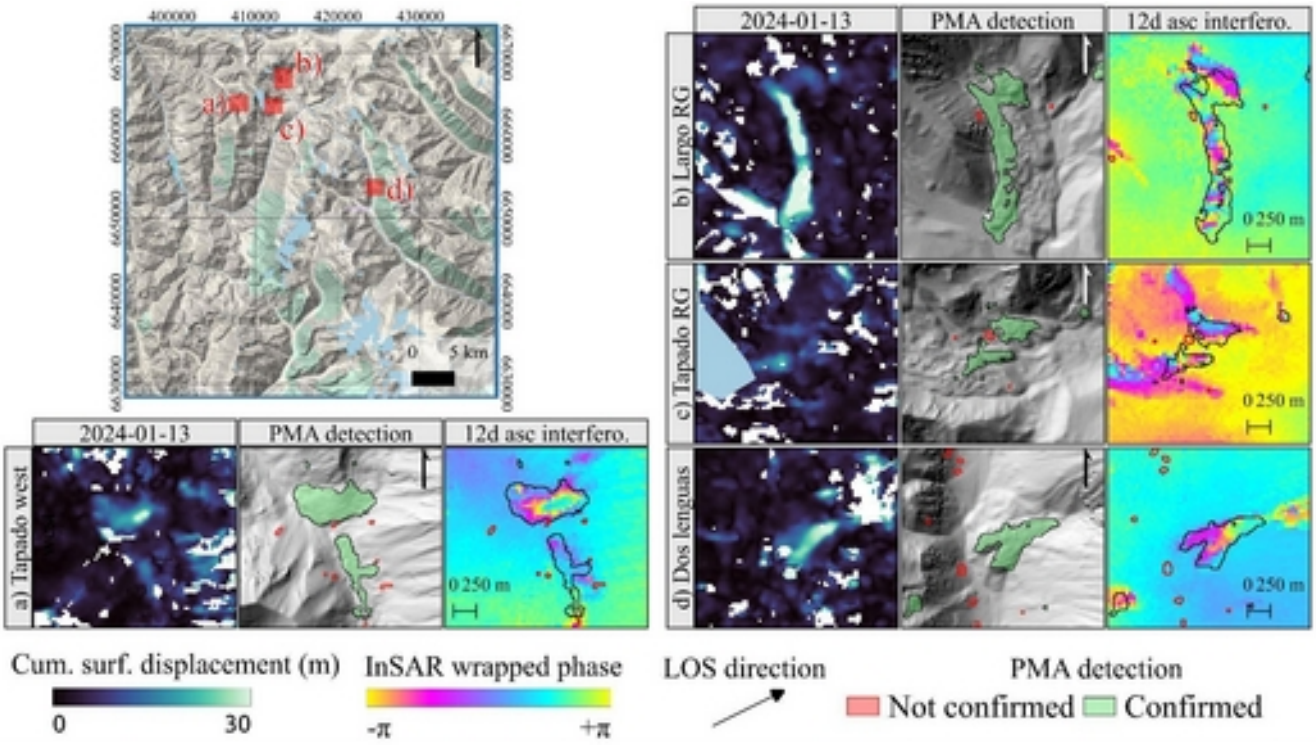

Figure 3: Example of raw outputs from inversion time-series, PMAs detection, and PMAs validation using InSAR wrapped interferograms. Upper left map shows the location of small inner maps a) Tapado west, b) Largo RG, c) Tapa dgo complex and d) Dos Lenguas. Image background corresponds to © GoogleTerrain. AFor all inner maps ~~from left to right~~, show cumulative surface displacement map (left) after inversion time-series (last date available). ~~In the middle,~~ PMA's detection after directional and magnitude filtering (middle) and ~~at right,~~ 12 days ascending S-1 wrapped interferograms (right). Red and green polygons represent raw 'non confirmed' and 'confirmed' PMAs, respectively.

4.4 Average spatial velocity and relative velocity changes

The a~~A~~verage velocity fields wasere estimated using a linear fit of the cumulative surface displacements per pixel though time. T~~hen, t~~he representative surface velocity was extracted for each confirmed PMA. The most common approach to obtain average representative surface velocity values is to use the most active portion, tyipically near ~~often situated in proximity to~~ the central profile (RGIK, 2023). This avoids the potential for lateral variability within the landform (Fig. 3). For instance, Kääb et al., (2021) ~~employ~~selected ~~a~~ small ~~area on the most~~ active sectors to ~~express the~~ representative the overall velocity of an~~for the~~ entire rock glacier. Nevertheless, ~~the selection of~~defining this 'active' area remains somewhat subjective and may vary between users. ~~In other respects~~Alternatively, Blöthe et al., (2020) proposed ~~the selection of~~ selecting pixels at the 95th percentile above the limit of detection (LoD) to ~~remove the~~reduce lateral effects. As shown in Fig.

3a to d, the pixels located in the borders often have values close to 0 ~~m a~~m yr^{-1}, due mainly to natural ~~geomorphological causes~~behaviour of rock glaciers~~ (i.e.~~ increased friction and low/no ice content in lateral margins~~)~~ as well as to window sizes of feature-tracking algorithms. So, the boundary effect for each PMA can bias the average velocity. To mitigate this bias, we propose a similar ~~metric~~approach ~~than~~o Blöthe et al., (2020)~~, to keep~~retaining only the Top 50% of pixels within each PMA (hereafter referred to as Top 50% average velocity) to better represent ~~the average~~ spatial velocity ~~for each PMA.~~ (cf. ~~Refer to~~ Section 6.3)~~. for a more detailed discussion.~~

Uncertainties of surface displacement and velocity fields were computed using the Normalised Mean Absolute Deviation (NMAD; Höhle and Höhle, 2009) over stable areas~~. Stable areas were~~ defined using TanDEM-X DEM and slopes ~~lower than~~ 35°. Glaciers outlines from RGI consortium (2017) and surroundings (~~, without taking into account neither glacier outlines~~ with a 500 m buffer~~) of 500 m for each glacier (RGI Consortium, 2017)~~ and~~nor~~ all PMAs~~, also not confirmed ones produced in this study~~ both confirmed and unconfirmed were excluded ~~(Fig. S4)~~. ~~In this sense, s~~Stable areas ~~correspond~~account for ~~to~~ 53% of the ~~entire~~ study area (i.e. ~~45~~x45 km²~~, (~~Fig. S4).

In this study, relative velocity changes between two periods are considered and can be calculated using Equation 1, by using the first period as the reference. The related uncertainties of the relative velocity change can be calculated using Equation 2, assuming that the NMAD for both periods ~~are~~is ~~not so different~~similar and not correlated (σV; cf. Section 5.4). Finally, from Eq. 1 and Eq. 2 we estimate a pixel-based relative velocity change and their related uncertainty, for each PMA.

$$V_{change} = \frac{V_2 - V_1}{V_1} \quad (1)$$

$$\sigma V_{change} = \sigma V \frac{\sqrt{\square}}{\square} \quad (2)$$

5 Results

5.1 Characterization of PMA extraction

Within the ~~area of interest covered by the~~ L7/8 dataset coverage area, the automatic PMA detection produced 1710 polygons of moving objects. ~~The r~~Raw PMAs area ranges from 225 to ~755,000 m² (Fig. 4). All PMAs were verified ~~based on~~using InSAR and optical cross-check validation (cf. Section 4.3). From this analysis, 29% of PMAs were classified as 'confirmed' (n~~b~~ = 501). ~~Within the 'confirmed' PMAs~~Among these, ~~we classified~~ 42% ~~of the PMA~~were identified as rock glaciers, 32% as landslides and 26% polygons ~~classified~~ as 'unclassified~~other~~'. Among the ~~42% of~~ rock glacier class~~s~~, we identified six rock glaciers directly connected to a debris-covered glacier. These remained ~~We decided to keep those within~~ in the 'rock glacier' class rather than creating a separate ~~class~~ category, as ~~because the~~ PMA ~~essentially~~ coverages was predominantly o~~nly~~ver the rock glacier component. Table 1 summarises all features and classes identified through the interpretation

analysis. ~~On the other hand~~Conversely, 71% of PMAs (n = 1209) were classified as 'not confirmed' ~~because~~due to a lack of ~~no~~ clear interpretation ~~could be obtained~~ from Google Earth optical imagery and interferograms. Among~~Within~~ the 'not confirmed' PMAs, 10% (n = 116) ~~of PMA~~ corresponds to ~~the~~ glacier class and ~~thus,~~were directly removed from the dataset. Table 1 summarises all features and classes identified through the interpretation analysis.

Table 1: Summary of raw PMA geomorphological characterisation through cross-check verification using S1 InSAR and Google Earth optical imagery (cf. Section 4.3). Information about their statistical distribution is presented in Figure S1.

TOTAL POLYGONS		Manual characterization		Above automatic surface threshold (2250 m² - 10 pixels)	
		n	%	**n**	%
Confirmation class	Geomoph class	1710	100	975	100
NOT CONFIRMED by InSAR	Sub total	1209	71	593	61
	unclassified~~Other~~	747	62	382	64
	valley bottom	159	13	77	13
	ridges	155	13	79	13
	landslide	17	1	14	2
	rock glacier	15	1	5	1
	glaciers	116	10	77	13
CONFIRMED by InSAR	Sub total	501	29	382	39
	rock glacier	211	42	153	40
	l~~L~~andslide	160	32	105	27
	unclassified~~Other~~	130	26	124	32

During ~~the~~ the manual characterization process, we noticed the presence of an important number of small and isolated polygons within the 'not confirmed' class (Fig. 4), mostly near~~often located close to the~~ mountain ridges and ~~at the~~ valley bottom (Fig. S3). As these tiny polygons ~~can~~could not be correctly interpreted, ~~we set up~~ a surface threshold of 2250 m² (i.e. 10 pixels)~~,~~ was applied to remove them automatically. This~~e~~ threshold ~~of 10 pixels has been~~was selected ~~on the~~ bas~~ed~~~~is~~ o~~f~~n the PMA size and ~~their~~ the corresponding InSAR fringe pattern (cf. Section 3.3; Fig. 3), as interpretation bec~~a~~~~o~~m~~e~~~~s~~ing difficult ~~to interpret~~ below this threshold. ~~By us~~Applying this ~~surface~~ threshold, 43% (n = 735) of ~~the~~ all PMAs were removed from the analysis.

The selected surface threshold ~~seems to be a good compromise to~~effectively removed noisy (smaller) PMAs while retaining ~~and keep~~ coherent (larger) PMAs, by only compromising 15% of confirmed PMAs (Fig. 4). After applying~~the~~ the surface threshold ~~is applied~~ and removing PMAs ~~corresponding to~~classified as glacier ~~class were removed~~, the remaining filtered

dataset containsing 901 PMAs (47% of the initial dataset), onlyof which 39% (n = 382) of PMA are confirmed. Thoese confirmed PMAs correspond to rock glaciers and mostly to large gravitational landslidesmass movements (among rock glaciersi.e., landslides and other mass movements; (Tab. 1). The confirmed PMAs havewith a mean surface area of ~30,000 m² (Fig. S3). The remaining 61% (n = 519) of not confirmed PMA also represent a consistent group of pixels, which potentially representsing a gravitational landslidesmass movement, but these could not be validated within the through cross-check methodology (cf. Section 4.3). Thoese unconfirmed PMAs have a mean area size of 8,000 m² equivalent to 35 pixels. aAnd are These polygons are often isolated and located close tonear the mountain ridges or at the valley floors. From Figure 4 we can also state that the ratio between confirmed andto not-confirmed PMAs increases whenith PMA are biggersize, suggesting that larger the objects size, the higher theare more likelyihood to be of PMA detectedion using the L7/8 dataset. Further discussion regarding the possible causes of these polygons can be found in Section 6.2. For the rest of the manuscript, we will only take into account the 382 confirmedvalid polygons (i.e. after applying the surface threshold) will be considered.

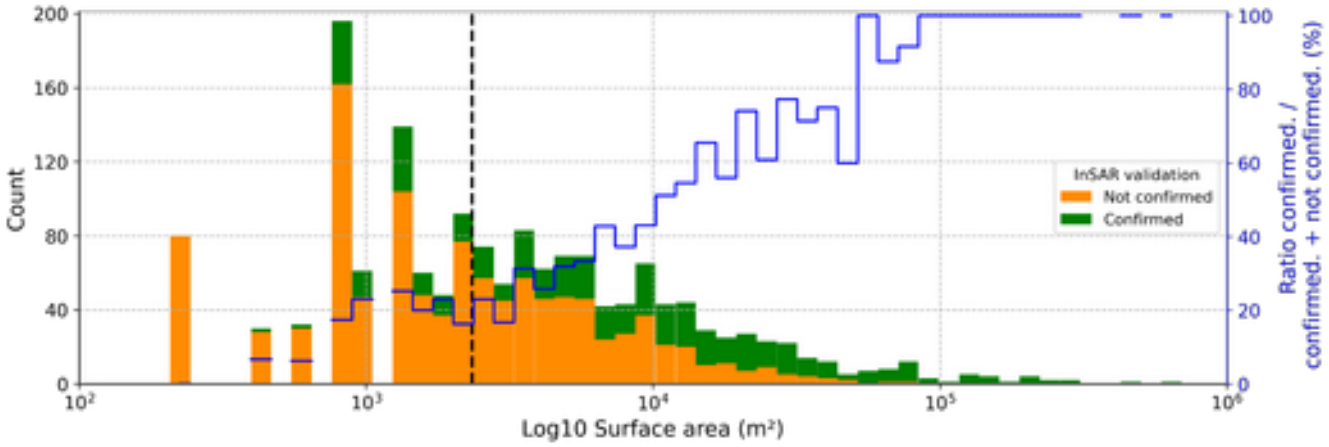

Figure 4: Distribution of raw 'confirmed' and 'not confirmed' PMA by surface area (bins = 50). Black vertical line represents the surface threshold i.e. 2250 m² (10 pixels) used as a filter to remove smaller PMAs. All polygons below the surface threshold were removed. Blue line, represents the ratio between confirmedvalid features over total features by bins. For access to our PMA polygons for our own assessment, refer to the Data availability section.

5.2 Regional distribution of surface velocity

Figure 5a provides an overview of the 24-year average velocity withinacross the central Andes region. For each PMA, we obtain a coherent downslopeward surface velocity field overlappings a sector of a rock glacier (cf. Section 6.3 for discussion). The Top 50% average velocity corresponds to 0.30 m am yr^{-1} over 24 years of displacements for all 382 PMAs.

The NMAD computed over stable areas corresponds to ±0.07 ~~m a~~m yr^{-1} over ~~24 years~~the same period (~~. Refer to~~cf. Section 5.4 for a discussion about the uncertainties).

The Top 50% average velocities ~~independent~~ for each geomorphological class —rock glaciers, landslides, and unclassified~~others~~— ~~correspond to~~are 0.37 ~~m a~~m yr^{-1}, 0.20 ~~m a~~m yr^{-1} and 0.18 ~~m a~~m yr^{-1}, respectively. ~~Among the classes,~~ R~~r~~ock glaciers ~~clearly show~~exhibit a median average velocity ~~higher (+~~23%~~)~~ higher than the ~~average velocity for the entire PMA~~ dataset~~-~~wide average (Fig. S9). Only three PMAs exceed ~~have~~ Top 50% average velocities greater than 2 ~~m a~~m yr^{-1} in Top 50% average velocities, corresponding to the Largo rock glacier (Fig. 2c; Fig. 5c), Olivares and Olivares west complex rock glaciers (Fig. 4f and g) and one landslide. Additionally,~~; and only~~ eight PMAs have ~~Top 50% average~~ velocities between 1 – 2 ~~m a~~m yr^{-1}, ~~corresponding to~~includ~~s~~ing five ~~relatively~~ large rock glaciers and three landslides. The ~~rest of the~~remaining 371 PMA~~s dataset (n = 371)~~ have~~has~~ average velocities below 1 ~~m a~~m yr^{-1} over 24 years.

In addition to ~~the~~ average velocity fields, ~~we were also able to obtain~~ cumulative displacement time series ~~(Fig. 5)~~were obtained for ~~of~~ all PMAs (Fig.5; Fig. S9) ~~over 24 years~~. These ~~displacements~~ time~~-~~series ~~are useful to depict~~capture temporal ~~changes~~ variations such as ~~changes in velocity, e.g.~~ accelerations or decelerations (Fig. 5e and f). Most of the rock glaciers ~~(those~~ with mean velocities < 1 ~~m a~~m yr^{-1}~~)~~, shows a linear trend ~~of~~in surface displacement~~s~~ (Fig. 5b and d). ~~Depicting a~~Annual velocity ~~changes~~fluctuations are ~~is rather challenging~~ difficult to assess ~~because~~ due to the high uncertainties ~~average NMAD for all individual velocity~~ of individual displacement fields~~pairs oin stable areas,~~ (NMAD between 1.21-3.07 m ~~which averages corresponds to 1.18 m am yr^{-1}~~ (Table 2). ~~In some cases, particularly for the fastest and bigglargest PMAs, qualitative assessment suggest some accelerations (Fig. 5e) and deceleration (Fig. 5f) could be qualitatively assessed. However, due to~~Given the large uncertainties at annual scale, the~~most observed accelerations are within the uncertaintiesuncertainitiesnot statistically significant for most of the PMAs (cf. Section 5.4).~~

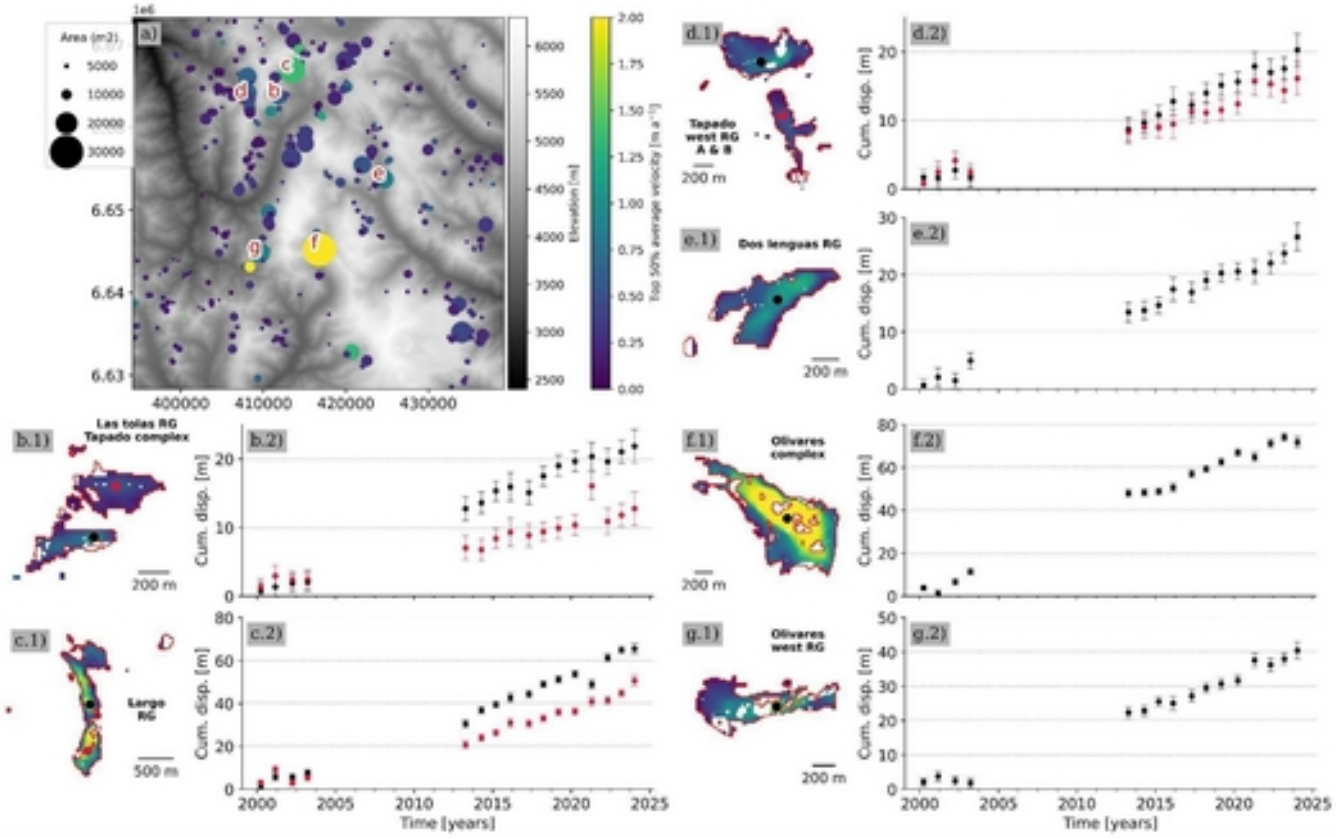

Figure 5: Surface kinematic characterisation for all PMAs in the central Andes region. a) Illustrates the spatial distribution of all valid PMAs (rock glaciers = 146; landslides = 115; unclassified~~others~~ = 103) coloured by the 'Top 50% average velocity' surface velocity (viridis colorbar) within the PMA surface. The size of the circle scales with ~~is proportional to the rescaled~~ PMA surface ~~in m²/1,000 for better visualisation~~. The red letters correspond to the study cases presented in the following subplots. The remaining subplots b) to g) (with a suffix of *.1) illustrate the mean annual velocity field over the 24 years (2000-2024) for a specific landform (name is displayed in bold), where the magnitude of velocity is coloured using viridis colorbar from panel a). Subplots with a suffix of *.2 represents the cumulative surface displacement time series in metres (subplots with a suffix of *.2), extracted on the black (and red) point within the landform. E~~Cumulative e~~rror bars show the ~~were computed~~ NMAD on stable areas for each date respectively (Section 5.4). Subplots b) to g) correspond to the following landforms b) Tapado Complex and Las Tolas Rock Glacier; c) Largo Rock Glacier; d) Tapado west Rock Glacier; e) Dos Lenguas Rock Glacier; f) Olivares Complex, g) Olivares west Rock Glacier.

5.3 Velocity validation using GNSS and VHR datasets

We compare surface velocity fields ~~in more detail~~ for the two selected sub-regions~~ around the~~ Tapado complex and Largo rock glacier (Fig. 2a). ~~A~~The first comparison ~~was made between~~involved GNSS points distributed along the main tongue of

Tapado complex and Largo rock glacier ~~—located in the central flow line as well as the borders of the landform—~~ and L7/8 and VHR surface average velocity fields~~. Both GNSS points and pseudo-GCPs are located in the central flow line as well as the border of the landform~~ (Figure 6). This point to pixel comparison is shown in Figure 7~~, from~~ where a good agreement between VHR and GNSS and pseudo-GCPs ~~exist~~is observed. However, s~~S~~ome ~~slight~~ differences ~~(i.e. —particularly an~~ underestimation of average velocity~~—) could be observed~~are noticeable~~ably on~~ a~~those~~ points ~~located on~~near the borders of ~~the~~ Tapado complex and Largo rock glacier. In addition, some of the fastest points on the Largo rock glacier ~~also present~~ show important differences. ~~Regarding specifically the comparison between L7/8 and GNSS datasets comparison, in the Tapado complex, both average velocities in the Tapado complex agree relativelyalign well (Fig. 7). However, fFor the Largo rock glacier, the difference in average velocity is important more pronounced becausedue to the average velocity field is moregreater heterogeneityceous of the velocity field. The pPoints located innear the borders do not fit with the pseudo-GCPs (cf. Section 5.4 for a quantitative assessment).~~

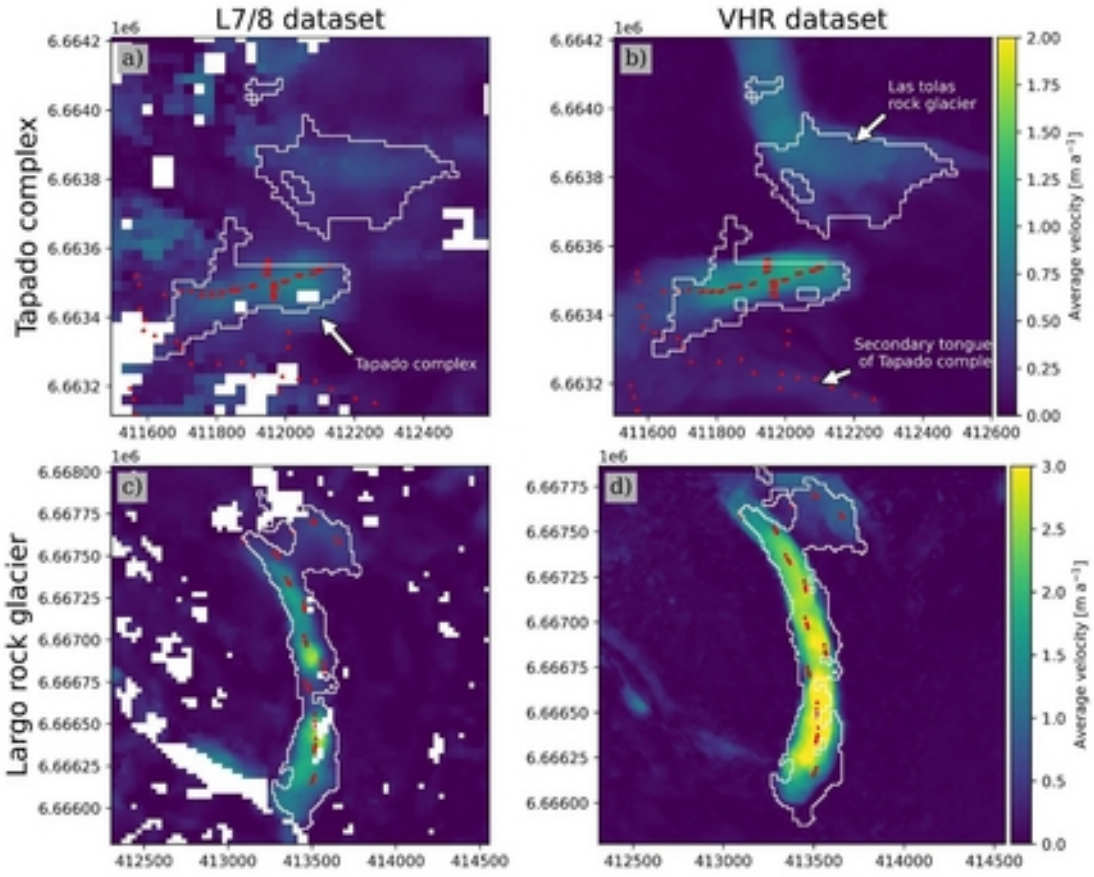

Figure 6: Comparison of mean annual velocity over the 2000-2020 period for Tapado complex a) and b); and Largo rock glacier c) and d) for both L7/8 and VHR dataset, respectively. Red points show the location of GNSS for Tapado complex

(CEAZA, 2023) and pseudo-GCP for Largo rock glacier. White polygons correspond to their respective PMAs identified from the L7/8 dataset (cf. Section 3.5).

Quantitatively, the average ~~differences in~~ velocity differences between VHR and GNSS points is ~~about~~ 0.01 ± 0.05 ~~m a~~m yr^{-1} (Tapado complex) and 0.38 ± 0.3 ~~m a~~m yr^{-1} (Largo rock glacier). Meanwhile, the average difference between L7/8 and GNSS points is 0.18 ± 0.24 ~~m a~~m yr^{-1} (Tapado complex) and 1.35 ± 0.84 ~~m a~~m yr^{-1} (Largo rock glacier; Figure 7). The good agreement on slow surface velocities on the Tapado complex could be explained ~~byto~~ by the homogeneous surface velocity field in both datasets (Fig. 6a). However, this consistency is not ~~the case on~~observed on~~at the~~ the Largo rock glacier, where large differences ~~could be~~are likely ~~explained~~due to ~~by~~ the heterogeneity~~ous~~ of its surface velocity field ~~from L7/8~~. Figure 6c shows a single PMA that could be either divided in two, splitting Largo rock glacier in two different units, with likely independent dynamics. This is not the case for the VHR velocity field, showing rather a more homogeneous spatial distribution of velocities (Fig. 6d).

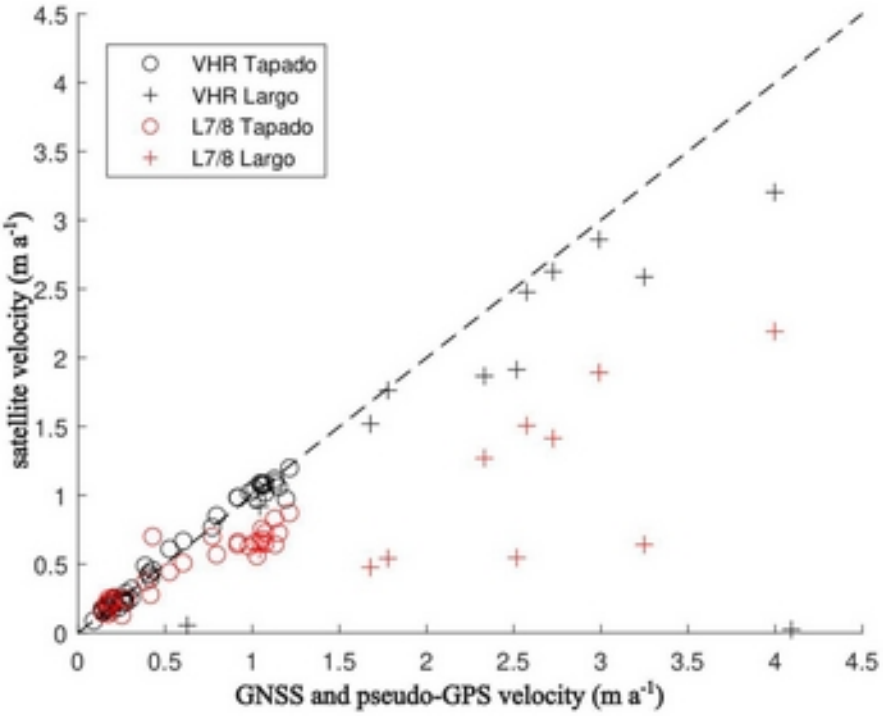

Figure 7: Comparison between GNSS (or, pseudo-GCPs) ~~points~~ average velocity and average surface velocity fields from ~~inversion time series for~~ both L7/8 (red) and VHR (black) datasets in the subregions of Tapado complex and Largo rock glacier. The average surface velocities from GNSS measurements, L7/8 and VHR datasets, were calculated according to the common time period, spanning from 2009 to 2020.

A detailed comparison with VHR optical imagery revealed a good agreement with GNSS data. The correlation coefficient between two datasets is ~~of~~ 0.99 for Tapado complex and 0.45 for Largo ~~was obtained for the Tapado and Largo~~ rock glacier~~,s~~ respectively~~, with and the coefficient of the~~ a linear fit ~~between VHR and GNSS~~coefficient of 0.99 and 0.44 ~~over the Tapado and Largo)~~respectively. The lower ~~values of the~~ correlation at Largo rock glacier is attributed ~~are due~~ to ~~those~~ points situated ~~in~~near the rock glacier borders (Fig. 6 ~~and ,~~ Fig. 7). The correlation between L7/8 and GNSS data is also very good, especially for the Tapado (0.92 and 0.7 for the Tapado and Largo respectively). However ~~but~~, L7/8 tends to always underestimate the velocities (coefficient of the linear fit of 0.69 and 0.45 for the Tapado and Largo rock glaciers). ~~In terms of velocity magnitude, the Tapado and Las Tolas rock glaciers exhibit minimaldo not present large differences. The L7/8 dataset tends to slightly underestimates surface velocities by up to 20% over those landforms. (cf.Please refer to~~ Section 6.1 for further discussion~~) about the possible causes of the underestimations~~.

5.4 Reported uncertainties

The horizontal accuracy assessment at annual and selected periods in this study is summarized in Table 2. For the L7/8 dataset, the average NMAD of ~~consecutive~~ surface displacement over stable areas obtained is 1.8 m in EW and NS components (Table 2~~Fig. 8~~~~). Uncertainties are slightly greater in recent years due to the cumulative error of time-series (Table 2).~~ which ~~The average median displacementvalue over stable areas~~ corresponds roughly to 1/10 of L7/8 pixel size. I~~For~~ individual displacements fieldsindividual~~consecutive annual~~ displacements~~surface velocities~~fields have too high uncertainties~~, the average NMAD is 1.18 m am yr^{-1}, making it. As expected, annual uncertainties are too high~~ to reliably detect ~~statistically~~ significant ~~changes in velocity at~~ annual scale velocity changes. However, a~~A~~t decadal time ~~spans~~scales, uncertainties decrease significantly (Table 2). The NMAD is 0.2~~+~~1 and 0.1~~93~~ ~~m a~~m yr^{-1}, for 2000-2014 and 2013-2024 periods, respectively. A~~gain, a~~~~A~~pplying the average NMAD value for both periods as a filter of PMAs, 150 PMAs are above this threshold, being good candidates to depict velocity changes. T~~Finally, as t~~he 'Top 50% average velocity' at decadal scale of all PMAs is 0.3 ~~m a~~m yr^{-1}, ~~at decadal scale and uncertainties encompasses~~ 1.5 times larger than the uncertainty~~43% of the overall average velocity~~.

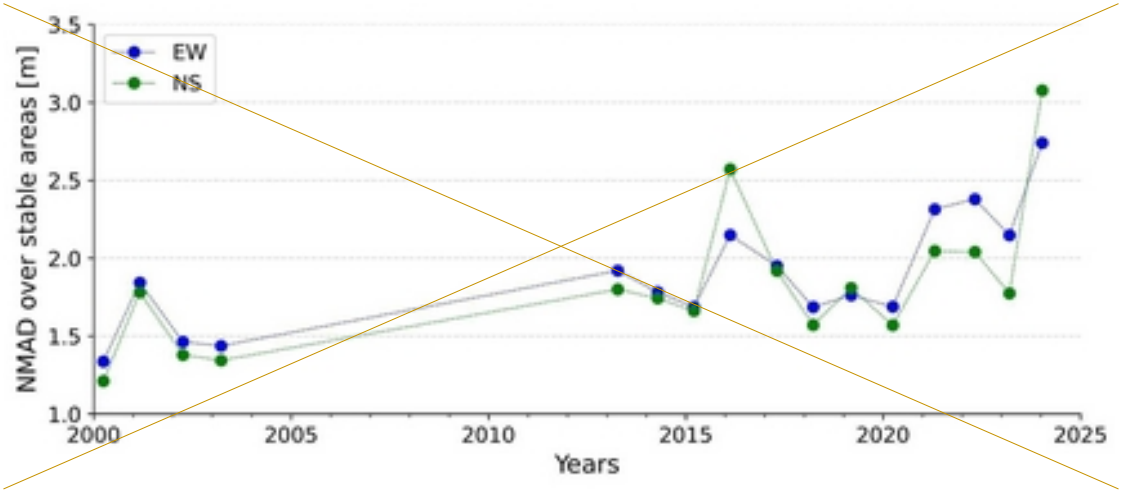

~~**Figure 8.** Annual NMAD values for the east-west (EW) and north-south (NS) components over stable areas for the L7/8 dataset. Figure S4 presents the stable area map of the study area used for NMAD computing.~~

Table 2. Accuracy and uncertainty assessment of surface displacement and surface velocity ~~maps~~ at annual and decadal time span. Spatial statistics were computed over a stable area of 53% for L7/8 (n pix = 4 810045), 55 % (n pix = 10 593 874) and 47% (n pix = 3 522 115) for Tapado complex and Largo rock glacier VHR dataset, respectively. [(a)] Values between brackets represent the range (min and max) values over a stable area for each component. [(b)] Difference velocity between GNSS and pseudo-GCPs vs surface velocity fields, computed using the same time period. [(c)] VHR dataset was split in two sub periods trying to fit the same time span as for the L7/8 dataset.

		STABLE AREAS								MOVING AREAS	
		Annual surface displacement [m] [(a)]		Decadal velocity [~~m a~~m yr^{-1}]				24-year velocity [~~m a~~m yr^{-1}]		Difference in velocity [~~m a~~m yr^{-1}] [(b)]	
				2000-2014		2013-2024		2000-2024		2010-2022	
		E-W	N-S	E-W	N-S	E-W	N-S	E-W	N-S	Tapado	Largo
L7/8 dataset	Mean	[-0.16, 0.45]	[-0.70, 0.20]	-0.009	-0.009	0.032	-0.021	0.004	-0.008	0.183	1.359
	Median	[-0.36, 0.32]	[-0.82, 0.34]	-0.006	-0.014	0.017	-0.023	0.004	-0.015	0.157	1.224
	Std	[2.25, 5.93]	[2.37, 6.03]	0.275	0.298	0.255	0.283	0.136	0.141	0.236	0.837
	Nmad	[1.33, 2.74]	[1.21, 3.07]	0.150	0.148	0.148	0.120	0.093	0.084	0.240	1.001
VHR		Multi annual surface		Decadal velocity				20-year		20-year velocity	

		displacement [m] (a)		[m a yr^{-1}] (c)				velocity [m a yr^{-1}]		[m a yr^{-1}]	
				2000-2014		2012-2020		2000-2020		2010-2022	
		E-W	N-S	E-W	N-S	E-W	N-S	E-W	N-S	Tapado	Largo
dataset	Mean	[-0.05, 0.11]	[0.19, 0.06]	0.010	-0.012	-0.002	-0.006	0.005	0.002	0.011	0.377
	Median	[-0.23, 0.0]	[-0.23, 0.06]	-0.011	-0.020	-0.002	0.000	-0.012	-0.012	0.006	0.206
	Std	[0.35, 1.34]	[0.31, 1.16]	0.120	0.097	0.049	0.054	0.078	0.065	0.047	0.307
	Nmad	[0.11, 0.36]	[0.28, 1.00]	0.030	0.078	0.030	0.010	0.020	0.048	0.036	0.133

5.5 Velocity changes

Using the 24-year surface displacement dataset, decadal velocity changes (Eq. 1) and velocity change uncertainties~~ity~~ (Eq. 2) were ~~analyzed by calculating surface velocities~~ computed using Top 50% average velocity over two periods: 2000–2014 (V_1) and 2013–2024 (V_2), ~~for~~across all PMAs. However, since relative velocity changes depend~~s~~ on the initial velocity magnitude (Eq. 1), velocity changes on PMAs with smaller magnitudes (<0.3 m yr^{-1}) exhibit higher uncertainties. According to our calculations, only 2% (n = 8) of the entire PMA dataset exhibits velocity changes greater than their respective uncertainties~~ity~~ (σV_{change};Fig. 9). Among these, 3 rock glaciers, 2 landslides, and 3 unclassified~~other~~ PMAs, were identified. These ~~1~~3 r~~R~~ock glacier PMAs have an average size of 60,075 m² (~27 pixels) with a Top 50% average velocity of 0.59 m yr^{-1}. ~~Six~~Two (~~five~~one) of them, ~~A~~acceleratetion (decelerate~~cion~~) with a mean value of~~averages~~ 198% (-46%) ~~in 6 (5) cases~~. Landslide PMAs have an average size of 15,412 m² (~69 pixels) and a Top 50% average velocity of 2.5 m yr^{-1}. However, only 2 cases exhibit acceleration with a mean of~~of~~ 214% ~~on average~~. PMAs in the 'unclassified~~other~~' class have an average size of 7,050 m² (~31 pixels) and a Top 50% average velocity of 0.44 m yr^{-1}. ~~Two~~One (two~~en~~) a~~A~~cceleratesion (deceleratesion) with a mean value of~~averages~~ 70% (-42%) ~~in 2 (10) cases~~. ~~The uncertainty in velocity change depends on the magnitude of velocity in both periods (Eq. 2). Smaller velocity magnitudes result in greater relative uncertainties (Eq. 2). To illustrate, a velocity increase from 0.5 to 1.0 m a^{-1} (100% change) has an uncertainty of 0.78 m a^{-1}, representing 78% of the relative change. In contrast, an increase from 1.0 to 2.0 m a^{-1} has an uncertainty of 0.39 m a^{-1}, or 39% of the relative velocity change. Consequently, only PMAs with velocities exceeding 1 m a^{-1} can be considered reliable for statistically significant velocity change. By considering PMAs with velocities exceeding 1 m a^{-1}, nine 'rock glaciers' and 2 'landslides'. Within those selected features, three rock glaciers showed an increase in velocity 11% (Fig. 5e), whereas six rock glaciers showed a decrease in velocity of 18% over two decades. On the other hand, two Landslides exhibited a larger increase in velocity of 50%. For further discussion, please refer to Section 6.5.~~

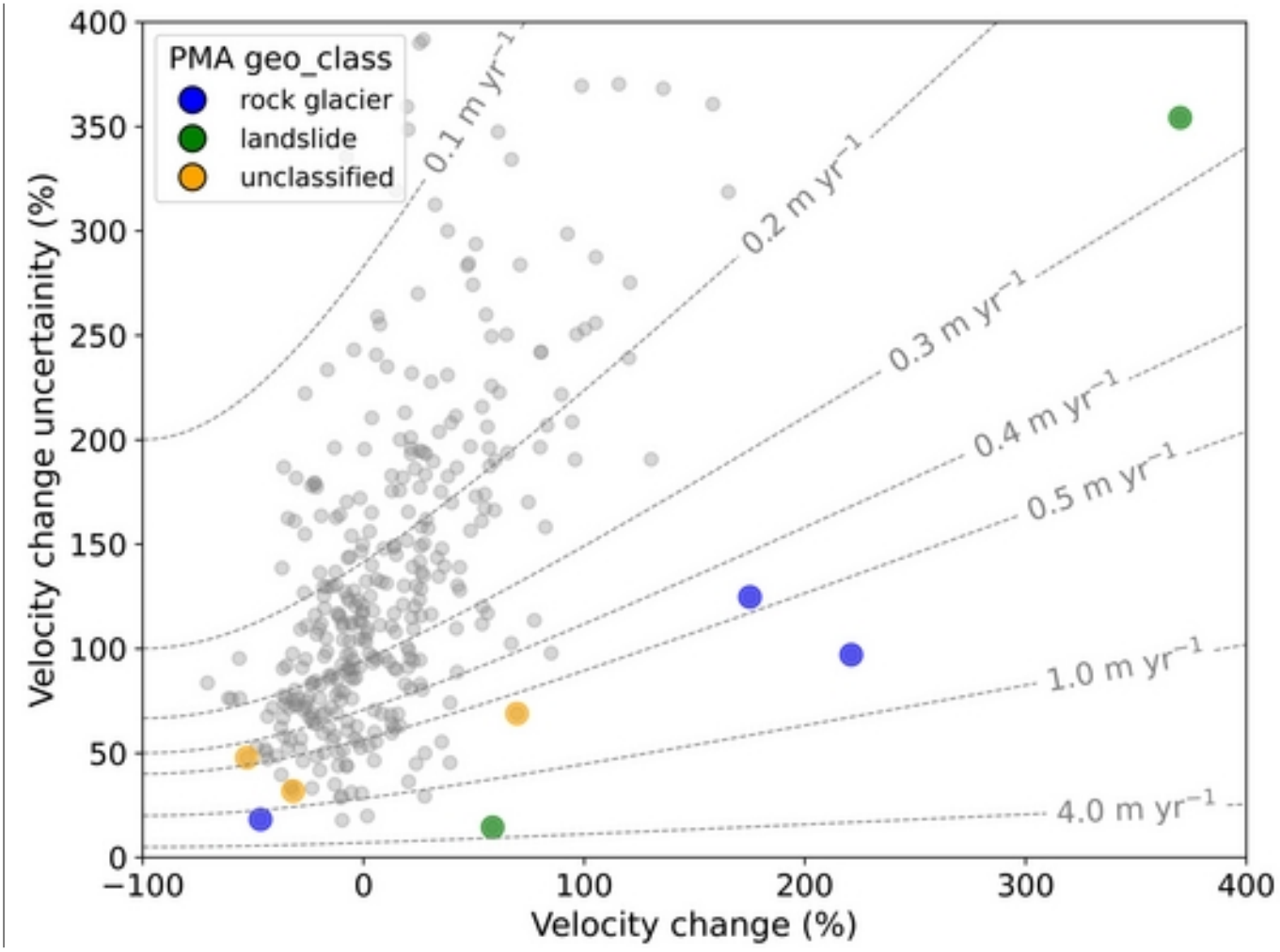

Figure 9. Modeling of relative velocity changes (~~ranging from -100% to 400%;~~ dashed lines; Eq. 1) and their respective uncertainties (Eq. 2) for various velocity magnitudes (0.1 – 4 m yr^{-1}). Grey dots represents the entire PMA dataset. B~~; while b~~lue, green and orange dots highlight PMAs ~~classified as rock glacier, landslide and other, respectively,~~ where velocity changes exceed their uncertainties~~y threshold~~.

6 Discussion

Rock glacier velocities are t~~y~~ypically estimated using high resolution optical data (e.g. Pellet et al., 2022) and SAR remote sensing imagery (Strozzi et al., 2020, Villarroel et al., 2018), but these datasets are prohibitively expensive for larger areas and/or ~~-~~relatively recent, covering only the past 20 years (Toth & Jóźków, 2016). In contrast, Landsat imagery (e.g. L4-5-7 or L8) extends back to the mid-1980s (Kooistra et al., 2024; Ustin and Middleton, 2021). ~~However, VHR and freely available SAR datasets are often limitedrestricted in accessibility and can be prohibitively expensive for larger areas.~~ In this

context, freely accessible L7/8 imagery emerges as a valuable source ~~of information~~ for studying rock glacier ~~dynamics~~ kinematics over extensive spatial and temporal scales (Lacroix et al., 2020b). To the best of our knowledge, this is the first time that Landsat imagery is being employed to monitor rock glacier displacement time-series and derive velocit~~ies~~ changes. This analysis is enabled by combining robust methods, including ~~redundancy of~~ information redundancy, ~~inversion of~~ time-~~-~~series inversion and the persistent moving area detection, which make L7/8 data viable for rock glacier monitoring. Nonetheless, ~~several aspects must be discussed in order to account for the~~ certain limitations and future~~, but also~~ perspectives regarding ~~of~~ the use of Landsat imagery for rock glacier kinematics analysis must be addressed.

6.1 Intrinsic limitations on the remote sensing datasets

The primary technical ~~point for~~ consideration is the spatial resolution of the L7/8 dataset (~~i.e.~~ 15 m in the panchromatic band). T~~Given that t~~heis pixel size is ~~relatively~~ coarse relative to the region's average surface velocity (i.e. ~1 ~~m a~~m yr^{-1}; Vivero et al., 2021; Halla et al., 2021)~~.~~, T~~t~~his method is therefore best suited for ~~large,~~ fast-moving rock glaciers. ~~Thus, i~~In ~~areas~~regions with ~~sizable~~large rock glaciers, such as the Andes or the High Mountain of Asia (Sun et al., 2024), medium-resolution L7/8 imagery can ~~can offer~~provide~~s~~ new insights into the temporal dynamics of rock glaciers. ~~However, its~~This ~~suitability largely depends on rock glacier size and pixel coverage within the landform (Section 5.1).~~ Here, a minimum surface threshold of 2250 m² (10 pixels) proves effective for the Andes but ~~perhaps~~may be less suitable~~so~~ for ~~other~~ regions with smaller rock glaciers, as the European Alps, wh~~ere~~~~ich~~ features may fall below the detection threshold. The 15 m spatial resolution also limits the ability to capture fine details, ~~making it challenging to discern~~thus small-scale spatial variations in velocity. Figure 6 illustrates how pixel size affects boundary delineation: in the Tapado complex, the secondary tongue (Fig. 6a, b) —moving at 0.25–0.5 ~~m a~~m yr^{-1} (Vivero et al., 2021)— appears indistinct~~,~~ ~~and shows~~with gaps and noise in displacement fields (Fig. 6a), as does the adjacent Las Tolas rock glacier. Despite this, the automatic PMA extraction (Section 3.4) successfully identifies a coherent PMA across much of Las Tolas' tongue (Fig. 6a), demonstrating this filter's potential for detecting active rock glaciers~~,~~ even ~~at~~in high altitude~~s~~, regions where snow and shadows introduce noise in image correlation (Cusicanqui et al., 2023).

Another key consideration is the surface roughness and texture of ~~the~~ rock glacier~~s~~, for instance features like ridges and furrows, which appear less detailed in L7/8 than in the VHR dataset~~. Surface features like ridges and furrows~~ (Fig. 2c)~~-~~. This can ~~both~~ impact the~~enhance or complicate image matching due to self-similarity, impacting~~ feature tracking performance (Kääb & Heid, 2012). For example, on the main tongue of the Tapado complex (Fig. 6a), L7/8-derived surface velocity is consistent with GNSS data (0.01 ± 0.05 ~~m a~~m yr^{-1}). While T~~t~~he 24-year average surface velocities align with Vivero et al., (2021)~~, but show~~ a discrepancy of 0.1–0.2 ~~m a~~m yr^{-1} is observed, likely due to L7/8's image resolution. Similar differences occur on the Dos Lenguas rock glacier, which has an average velocity of 1.5–2 ~~m a~~m yr^{-1} (Halla et al., 2020; Strozzi et al., 2020), while L7/8 imagery shows average velocities of 1.1–1.5 ~~m a~~m yr^{-1} (Fig. 5e). In contrast, Largo rock glacier presents ~~more~~greater complexity. Despite its ridge-and-furrow morphology, its homogeneous texture (Fig. 2d) ~~limits~~reduces contrast,

potentially explaining observed discrepancies between the L7/8 and VHR results ~~for average surface velocities~~ (3–4 ~~m a~~m yr$^{-1;}$ Figure 6b). ~~The resolution of L7/8's imageslower resolution, which capture~~s ~~less surface detail~~s, ~~affects~~ Vvelocity estimat~~esions with~~in landforms with high spatial heterogeneity~~internal variability~~ are highly affected by the L7/8 resolution, which captures less surface details. Therefore, ~~the choice of~~ correlation parameters are key when performing image correlation (Kääb & Heid, 2012; Leprince et al., 2008; Rosu et al., 2015). As L7/8's smallest matching window (3x3 pixels, covering 2025 m²) differs substantially from the VHR window (7x7 pixels, covering 49 m²) leading to an averaging effect. This difference contributes to the observed variability ~~within the same~~ in features ~~like~~such as Largo rock glacier. Finally, ~~changes in~~ solar illumination changes~~can~~ introduce shadow-induced noise in image correlation (Dehecq et al., 2015), which w~~e~~as minimized by selecting L7/8 images mainly from March (with a few from January).

6.2 Validation of PMA using InSAR and local rock glacier inventories

The average velocity fields from L7/8 optical satellite data align ~~reasonably~~ well with Sentinel-1 interferograms and their interpretation (~~–~~Fig.~~ure~~ S9) ~~visually~~ when comparinges InSAR wrapped interferograms and PMA characterisation. However, this comparison is affected by different uncertainties: (i) w~~W~~hile S1 interferograms show only LOS motion, limiting the discrimination of lateral and vertical movements (Barboux et al., 2014), optical imagery provides both horizontal components of surface kinematics; (ii) ~~Regarding the binary classification (i.e. 'confirmed' and 'not confirmed'), PMAs are based on quantitative measurements, though ; however, there is uncertainty/ambiguity in the InSAR activity classes and PMA velocity range classifications. First, sSome PMAs cover complex landforms with diffuse boundaries, and thus were assignedrequiring a general geomorphological classification without specific discrimination, including debris-covered glacier and glacier-rock glacier transitions (Monnier & Kinnard, 2015, 2016). SecondAdditionallyAdditionaly, PMAs categorized as 'other' geomorphological classes lack clear geomorphological features for fullcomplete interpretation~~. Not confirmed PMAs, often located in low-relief areas, near riverbeds, or close to ridges (Fig. S2), are likely due to the smoothed DEM used as slope direction reference or shadows in L7/8 images. Some ~~other~~ PMAs ~~were found~~ also appear near human settlements, including mining sites, where InSAR did not indicate displacement;~~–~~

~~The combined use of radar and optical data at the time of classification influences the assigned velocity class.~~ (iii) Interferograms reflect movements over short time intervals (e.g. 12 days,or 60 days, etc) within a limited time-period (2022-2023), potentially missing gravitational movements that were inactive at that time; (iv) InSAR velocity classes for ~~each~~ PMAs ~~were assigned~~ follow~~ed~~ing RGIK (2023) recommendations, though FLATSIM interferograms have a coarser pixel size (~~i.e.~~ 30 m) than those in Stro~~z~~tzi et al., (2020) or Bertone et al., (2021), ~~sometimes~~ making fringe patterns ~~barely discernible~~difficult to discern, specially for small landforms. ~~In a~~ (iii) ~~Additionally, interferograms reflect LOS movements over short time intervals (e.g. 12 days,or 60 days, etc) within a limited time-period (2022-2023), potentially missing gravitational movements that were inactive at that time.~~

Some PMAs cover complex landforms with diffuse boundaries, and thus were assigned requiring a general geomorphological classification without specific discriminations, including debris-covered glaciers and glacier-rock glacier transitions (Monnier & Kinnard, 2015, 2016). Additionally, PMAs categorized as 'unclassified' geomorphological classes lack clear geomorphological features for a complete interpretation.

Rock glaciers are slightly better detected than ~~other features like~~ landslides, likely due to the lower motion variability with time ~~over time~~. ~~Indeed, r~~Rock glaciers are viscous flows (Haeberli et al., 2006) ~~that face changes of~~ undergoing activity changes over long periods ~~of time~~ (Kellerer-Pirklbauer et al., 2022; Lehmann et al., 2021). ~~On the~~In contra~~stry~~, landslides ~~can be~~ are influenced by seasonal and transient patterns (Lacroix et al., 2020b).

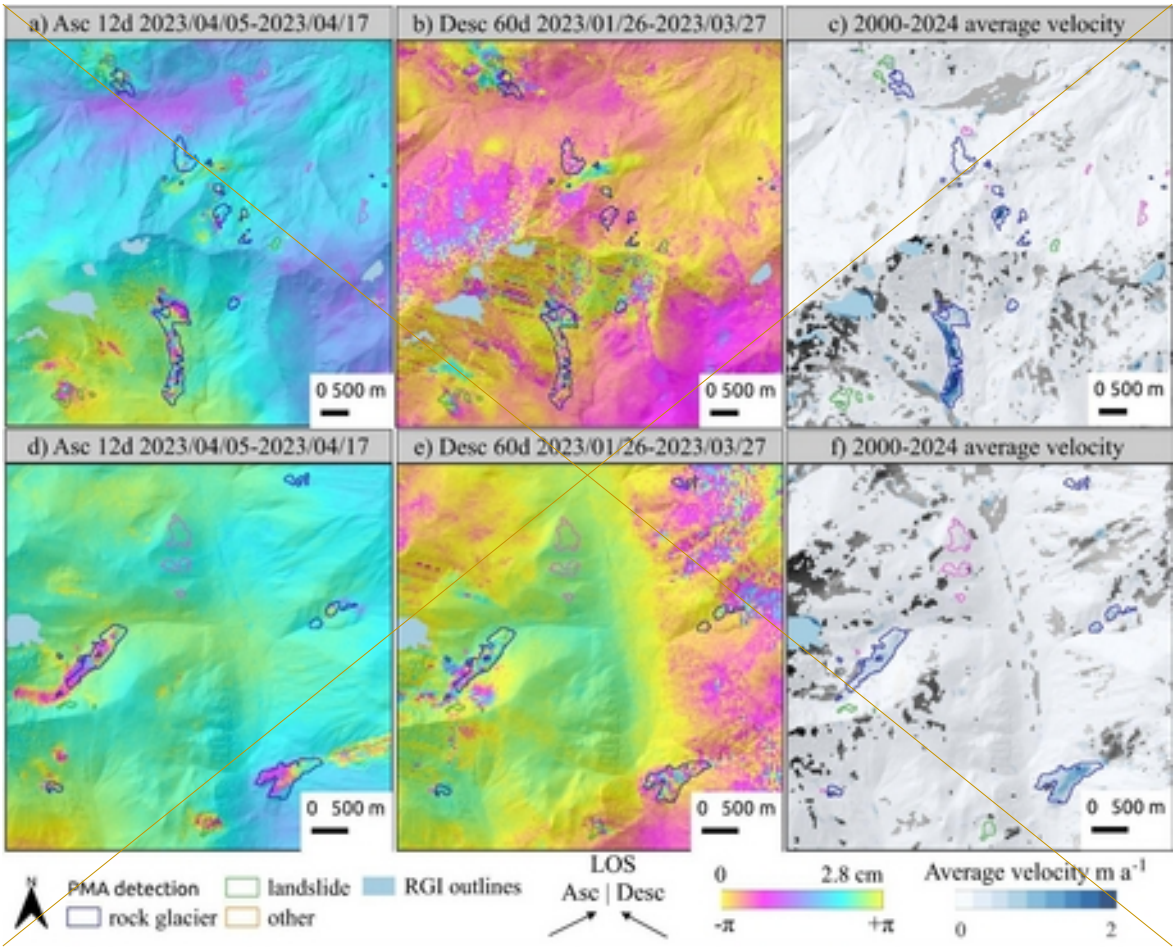

~~**Figure 9:** Comparison between Sentinel-1 wrapped interferograms at 12 and 60 days of interval and average surface velocity fields, in two small regions in the Central Andes.~~

A comparison ~~was conducted between the two~~ with existing rock glacier inventories for the Chilean (DGA, 2022) and Argentinian (IANIGLA, 2018) Andes was conducted~~,~~ focusing~~focussedding~~ on PMAs classified as rock glaciers only (n~~b~~ = 153). Using Ch-Arg rock glacier inventory as a reference, 68% of the PMAs (n~~b~~ = 104) intersects the existing inventory at an average of 30% of their surface area (Fig. S12). However, only 20% of the overlapping PMAs (n~~b~~ = 20) ~~overlaps~~coincide with ~~the inventory by~~ more than 50% of their surface. The remaining 32% of the PMA (n~~b~~ = 49) ~~comprises~~ are unmapped rock glaciers identified through L7/8 optical imagery and validated with InSAR (RGIK, 2023). This comparison relies on the accuracy of the Ch-Arg rock glacier inventories, which contains certain ambiguities. For instance, the Chilean inventory, released in 2013 and updated in 2022 (DGA, 2022), ~~shows an~~ overrepresent~~sation of the~~ rock glaciers by including ~~some~~ headwall sections (Fig. S12), while the Argentinian inventory defines rock glacier ~~limits~~boundaries more conservatively. Neither of the two inventories has yet been updated ~~yet in~~ according~~ance with~~ t~~ohe~~ RGIK guidelines (RGIK, 2023). Finally, ~~regarding the~~~~for PMAs activity class classified as rock glaciers,~~ InSAR velocity data indicate that 69% of the rock glacier PMAs (n~~b~~ = 105) were detected using 12-day interferograms (Fig. ~~9f~~S16), suggesting a velocity class between 30–100 c~~m~~ ~~a~~m yr^{-1} (RGIK, 2023), ~~which agrees~~ consistent with our results~~thise study's findings of this study~~.

6.3 Average PMA surface velocity

Since our dataset ~~compris~~provides a spatial representation of surface displacement ~~field~~ for 382 PMAs~~ (~~comprising 153 rock glaciers, 124 landslides and 105 non-classified landforms~~),~~ we ~~can~~ pose the following question: what is the most appropriate threshold for computing average surface velocity fields?

~~In our study, c~~Computing statistics per landform using the same threshold ~~could be complex~~is challenging~~,~~ due to the large pixel size of L7/8 imagery and the ~~size of~~varying PMA sizes. ~~If we compute~~When spatial average velocities are computed using the Top 50% pixels, ~~the~~ bias resulting from lateral variability is ~~automatically removed~~minimized, and ~~an area in~~only the ~~middle~~central portion of the PMA is conserved (see Fig. S15 for a comparison), corresponding to the fastest area (Fig. 6). This ~~fastest area obtained from this~~ methodology inspired from ~~(~~Blöthe et al., (2021) ensures that the fastest area is selected independently~~independent~~ for each PMA ~~area and is solely~~ based solely on 24-year average velocity~~ within the PMA~~. However, ~~when computing spatial average velocities~~ using different thresholds~~;~~ can lead to ~~the mean average velocity may be~~ overestimation~~sted~~ of average velocity. Figure 10 ~~also presents a~~ quanti~~fiestative estimation of~~ the i~~mpact~~n~~fluence~~ of selecting 'Top 50%, 30% and 10% average velocity. The mean difference between the ~~average velocity over the entire~~ full-PMA average velocity~~surface~~ and the 'Top 50%, 30% and 10% ~~average~~ velocit~~iesy~~' corresponds to 20%, 31% and 44%, respectively. These differences underscore the significance of selecting ~~the most~~an appropriate threshold~~s~~. Here, we consider that the 'Top 50% average velocity' computed over a 24-year period represents an ~~the~~ optimal compromise ~~between the~~ preserving average velocity field while minimizing~~without~~ lateral effects and maintaining a sufficient number of ~~the remaining amount of~~ pixels ~~representation~~ within the PMA. This approach also~~, with the potential to~~ reduces the ~~ambiguity~~

introduced by the operator-induced ambiguity. Nevertheless, further studies should be conducted to evaluate this metric using different temporal intervals and with different remote sensing datasets.

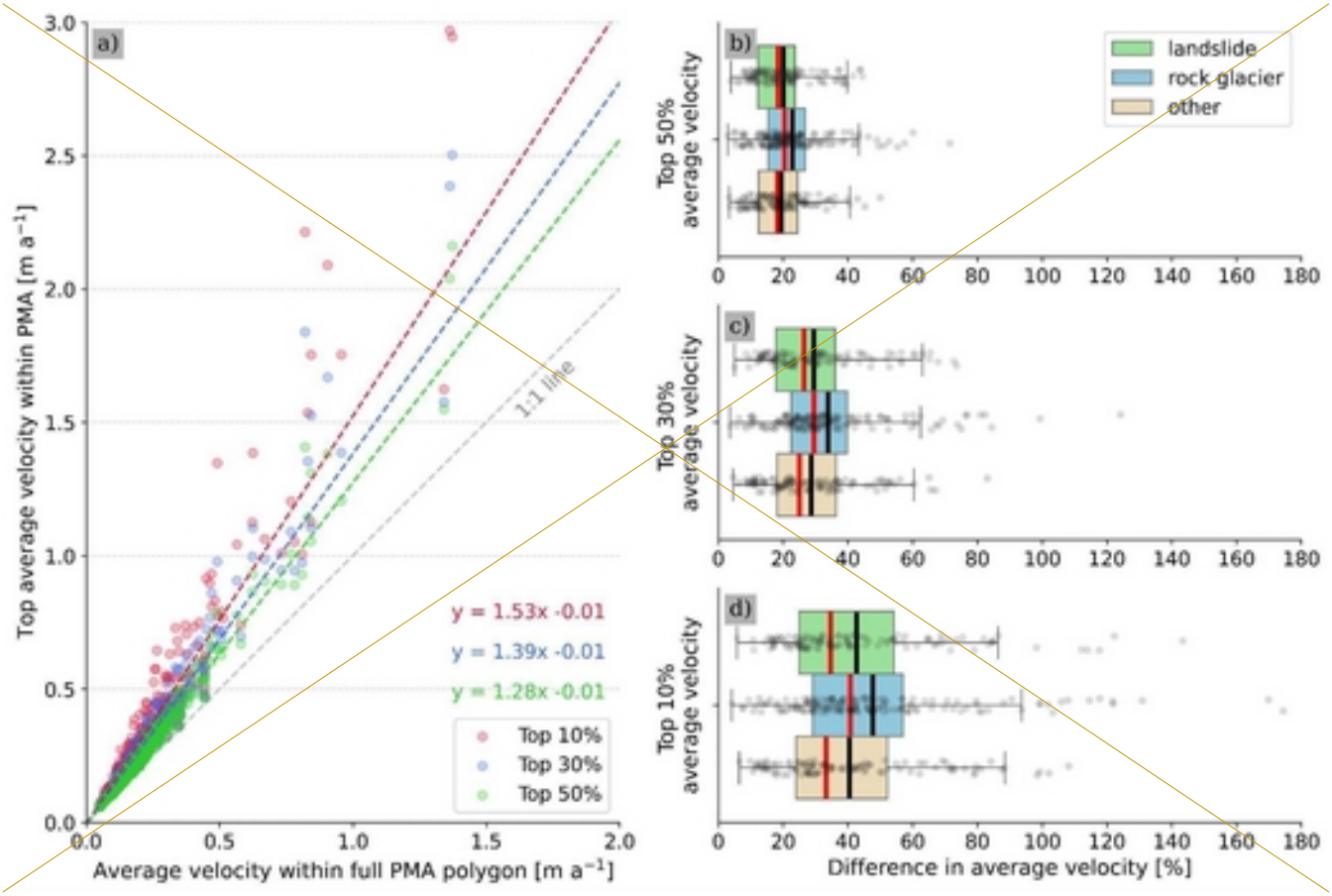
a)
b)
c)
d)
Top average velocity within PMA [m a^{-1}]
Average velocity within full PMA polygon [m a^{-1}]
1:1 line
y = 1.53x -0.01
y = 1.39x -0.01
y = 1.28x -0.01
Top 10%
Top 30%
Top 50%
Top 50% average velocity
Top 30% average velocity
Top 10% average velocity
landslide
rock glacier
other
Difference in average velocity [%]

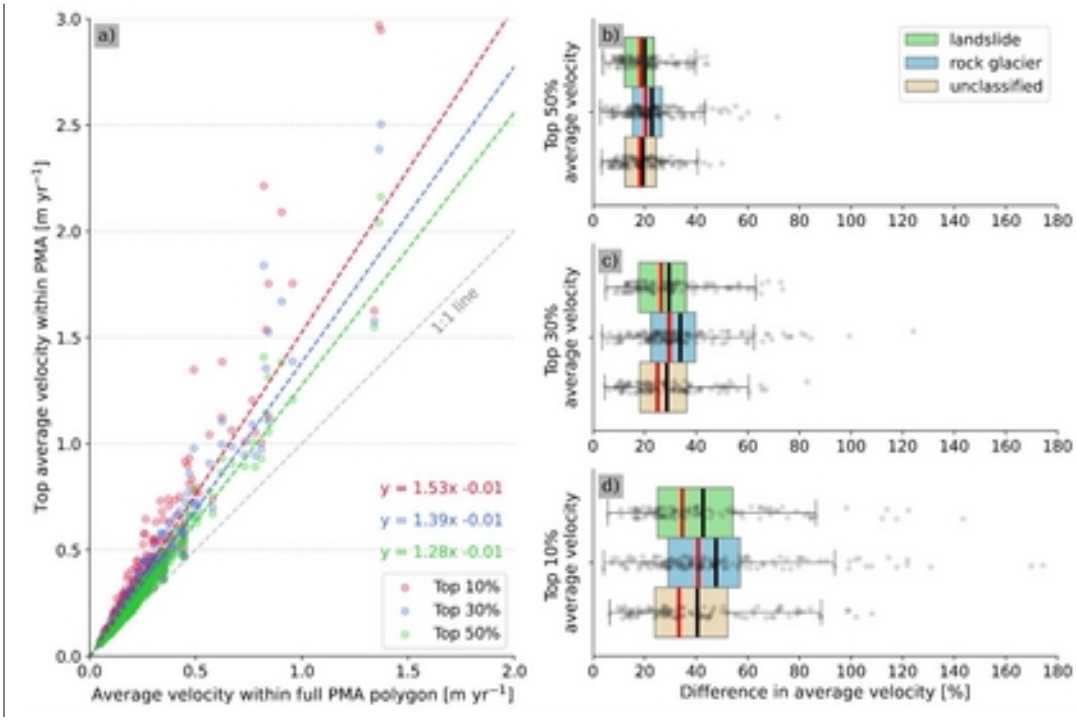

Figure 10: a) Comparison between average velocity computed using the entire PMA surface and 'Top 50%, 30% and 10% average velocity' within PMA. Subplots b), c), and d) show the difference of average velocity 'Top 50%, 30% and 10% average velocity' within respect to the average velocity computed over the entire PMA surface.

6.4 Surface velocity variations and uncertainties

Regarding uncertainties in those PMA with GNSS data—Tapado and Largo rock glaciers—our approach generally underestimates surface velocities by 10–20% on average (Fig. 7). Tapado surface velocities (1–2 m am yr^{-1}) align well with GNSS data, butwhereas Largo surface velocities (2–4 m am yr^{-1}) are underestimated by 30–40%, likely due to textural differences and lack of contrast on L7/8 dataset (Section 6.1). The overall underestimation of surface velocities in L7/8 imagery could be attributed to the large pixel size (15 m), which reduces pixel counts per matching window. Additionally, data gGaps between 2003 and 2013 may also introduce biases in displacement time series. Velocities were validated oOnly on two of the 382 PMAs were validated using in situ measurements or VHR imagery, raising questions about the validity of the remaining rock glaciers measurements. Calculations show an NMAD of surface velocities over 24-year onver stable areas of 0.07 m am yr^{-1} ± 0.16 as standard deviation (1σover 24-year period), similar to the uncertainties found by Kääb et al., (2021) in the Tien Shan region using high-resolution historical images with poor scan quality. In contrast, Blöthe et al., (2021), using a Limits of Detection (LoD) method with high-resolution optical images, reported uncertainties from 0.28 to 0.5 m am yr^{-1}. The low uncertainties reported in thefrom L7/8 imagery, computed over a 24- years period support the deliability of , brings confidence in theour interpretation.

However, annual velocity uncertainties are notably higher than those estimated over the entire period (Table 2~~Fig. 8~~). The ~~mean ± standard deviation~~ NMAD of consecutive displacements over stable areas (Fig. S3) ~~for consecutive displacements~~ is 1.8 m ± 0.33 ~~and 1.18 m am yr^{-1} ± 0.44~~, consistent with ~~values reported in~~ previous studies (Lacroix et al., 2019; Scherler et al., 2008), using L7/8 images. ~~Applying this mean NMAD as LoD filter (Blöthe et al., 2021) o~~Only 2% of PMAs (n = 8) ~~above the threshold~~ were retained~~,~~ by applying this NMAD as LoD filter (Blöthe et al., 2021), corresponding to large and fast rock glaciers (Fig. 5c, f, and g). This analysis demonstrates that L7/8 imagery allows kinematic characterization of rock glaciers over large periods of time (10-20 years) but not for annual velocity variations. ~~Further studies are required to enhance our understanding of the annual velocity changes observed using L7/8 images.~~

Regarding d~~D~~ecadal velocity changes uncertainties between 2000-2014 and 2013-2024 ~~, (Eq. 1) raise questions about the representativeness given velocity uncertainties (Eq. 2).~~ t~~T~~hree main factors contribute:

- **Observation discrepancies:** The 2000~~ to~~ 2014 period includes only six images~~years of observations~~ due to a gap between 2003 and 2013, whereas 2013 to 2024 has 11 years of continuous observations. This imbalance may bias ~~the~~ average velocity ~~for each period,~~and conditioning related uncertainties (Fig. 5). ~~The u~~Using~~e of~~ ASTER ~~images~~ or other medium-resolution ~~data~~imagery could help to fill this gap, despite its~~the~~ low radiometric resolution (Lacroix et al., 202~~0~~).

- **PMA size:** L7/8 imagery performs better on larger landforms with more ~~moving~~ pixels. ~~As high uncertainties of v~~Velocity change uncertain~~i~~ties are higher at PMA~~are present on~~ borders ~~of PMAs~~ due to the ~~small~~lower velocity magnitudes and the lateral discontinuity~~, the~~~~but the border effect is~~, less pronounced on bigger PMAs ~~than the smaller ones~~. However, larger PMAs obtained in this study are ~~landforms related~~linked to complex processes (e.g. glacier-permafrost interactions) which may have ~~been~~ influenced ~~by~~ internal landform variability. The Largo rock glacier ~~experienced~~ exhibits ~~a change in~~ a velocity increase of +54% and +29% in L7/8 and VHR datasets, respectively. Conversely, the Olivares ice-debris complex (debris-covered glacier connected), showed a -9% velocity change in one decade using~~the~~ L7/8 data. Similar patterns ~~observed~~ were observed 100 km south o~~f~~f Elqui valley (Monnier et al., 2014; Monnier and Kinnard, 2013, 2015), as well as in the Tien Shan region (Kääb et al., 2021), the European Alps (Cusicanqui et al., 2023; Gärtner-Roer et al., 2021; Kunz and Kneisel, 2020). ~~All t~~These observations suggest that complex interactions between glacier retreat and permafrost-related landforms influence surface velocities ~~in contiguous landforms~~, highlighting the need~~areas~~ for further research.

- **Andean velocity observations:** Limited Andean studies report ~~few~~significant velocity changes in recent decades. Vivero et al., (2021) found a 7% of acceleration in the 2000-2020 decades. Our VHR data ~~show~~ show limited changes, with -3 ± 10 % slow-down in the Tapado ~~rock glacier~~complex and +14 ± 10 % speed-up in Largo rock

glacier between 2000-2010 and 2010-2020. Over 40 years, Vivero et al. (2021) observed a 0.2 ~~m a~~m yr^{-1} acceleration in Tapado ~~rock glacier~~complex, representing a 25% ~~of velocity~~ increase in ~~average~~velocity. Such a level of acceleration might not be detected by L7/8 imagery due to the too low velocity. Further studies could benefit from incorporating of older datasets, like SPOT 1-4 up to the mid 1980's or Corona images from the 1960s (Dehecq et al., 2020; Kääb et al. 2021).

6.5 Wider geomorphic implications of PMAs

Understanding the broader geomorphic implications of PMAs is critical for interpreting their role ~~within~~in high mountain environments and their response to climatic and geomorphological processes. While this study primarly ~~much of the manuscript~~ focuses on kinematic and spatial characteristics of PMAs, this section ~~aims to~~ contextualizes the observed patterns within a regional framework.~~;~~ By bridging findings with topographic and geomorphological contexts, we ~~shedding~~high~~-~~light ~~on~~ the factors influencing PMA~~their~~ spatial distribution and surface dynamics. The PMAs in the study area show heterogeneous spatial distribution across topographic conditions (Fig. 5a). Analysis of the Top 50% average velocity ~~and its~~in relation~~ship~~ to slope, aspect, elevation and surface area~~—~~derived from the TanDEM-X 12.5 m DEM~~,~~ ~~—~~ reveals several key patterns (Fig. 11, Fig. S7)

- Rock glaciers predominantly occur~~are generally found~~ uniformly on slopes of 10–35°, while 'landslides' and 'unclassified~~other~~' features are concentrated on slopes steeper slopes ~~(than~~ ≥25°), peaking at 30° and 35°, respectively. This pattern aligns with the regional slope distribution, suggesting slope as a key control ~~of slope~~ for landslides and unclassified~~other~~ landforms (Fig. 11a).
- Slope aspect ~~distributions~~ varies~~y~~ distinctly ~~between feature~~by landform type~~s~~. Rock glaciers primarily face West to South and East, consistent with regional permafrost models (Gruber, 2012, Obu, 2021; Azocar et al., 2017). In contrast, landslides and unclassified~~other~~ features ~~are~~ predominantly occur on northwest to east~~-~~facing slopes (Fig. 11d). Similar findings from Blöo~~o~~thcë et al., (2021) in the Cordon del Plata ~~also emphasize~~underscore slope orientation as a key controlling factor.
- Most ~~of the~~ rock glaciers with velocities between 1–2 ~~m a~~m yr^{-1} are located at ~~altitudes of~~ 4,500–5,000 m a.s.l., although no strong correlation with altitude was found. ~~In contrast~~Conversely, 'landslide' and 'unclassified~~other~~s' PMAs occur at lower elevations (~~around~~ ~3500 m a.s.l.), often where ~~the presence of~~ permafrost is heterogeneous or discontinuous (Gruber 2012; Azócar et al., 2017) (Fig. 11b).
- In the Top 50% average velocity category, larger rock glaciers exhibit higher surface velocities, unlike 'landslide' and 'unclassified~~others~~' ~~categories~~PMAs (Fig. 11c). This may reflect specific and local geomorphological ~~context~~conditions, such as the accumulation zone at Largo rock glacier, ~~which likely drives~~where material influx

likely drives (Janke and Frauenfelder, 2008) ~~and~~ surface acceleration (+54% in the L7/8 dataset) (Janke and Frauenfelder, 2008). By contrast, Olivares ice-debris complex shows deceleration, potentially linked to ice-mass loss in adjacent debris-covered glaciers. Similar patterns have been observed in the Tien Shan region (Kääb et al., 2021) and more recently in the European Alps (Manchado et al., 2024). ~~More detailed~~Further studies are necessary to understand the mechanics of these complex landforms.

Although ~~the objective of our~~ this study focuses ~~is the~~on monitoring ~~of~~ rock glaciers on a regional scale, it also identifies other PMAs corresponding ~~to mass movements such as~~ to landslides and some unclassified landforms ~~could also be identified~~. Our results suggest possible correlations between gravitational movements in high mountain areas (e.g. Haeberli et al., 2017; Patton et al., 2019) and permafrost degradation (i.e. freeze, thaw of permafrost) in recently deglaciated areas (Pánek et al., 2022). This study ~~allows us to complete those~~contributes to existing mass movement inventories in the region (e.g. Iribarren Anacona et al., 2015), highlighting areas for further research. While these findings provide valuable~~suggest useful~~ regional insights ~~relationships between~~ into surface kinematics and topographic relationships~~parameters at the regional scale~~, they must be interpreted cautiously. The morphological statistics here are derived ~~only within~~solely from PMA boundaries and may not fully represent ~~the whole~~ entire~~entier~~ landforms (Fig. S12). Additionally, PMAs exclude feeder basins, responsible for material ~~supply~~ and water supply to the rock glacier (Blöthe et al., 2021; Cusicanqui et al., 2021). Further studies should be conducted to look at the influences of feeder basins on surface kinematics of rock glaciers.

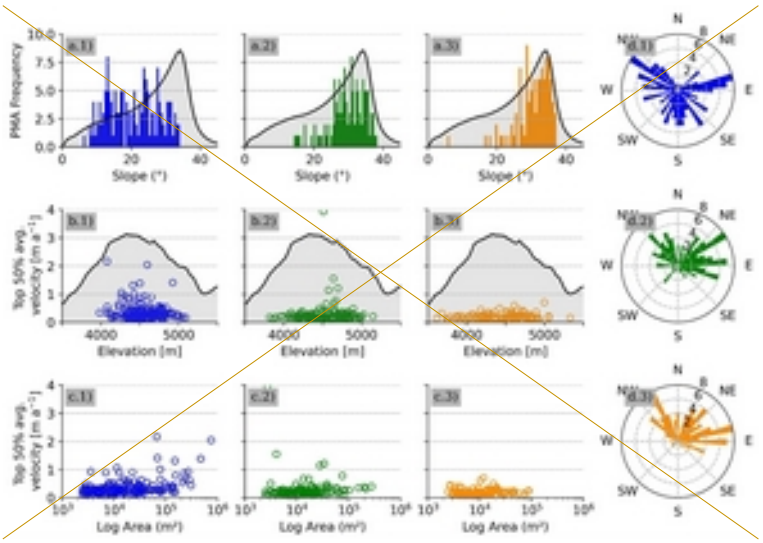
a.1)
a.2)
a.3)
d.1)
b.1)
b.2)
b.3)
d.2)
c.1)
c.2)
c.3)
d.3)
PMA Frequency
Slope (°)
Top 50% avg. velocity [m yr⁻¹]
Elevation [m]
Log Area (m²)
N
NE
E
SE
S
SW
W
NW

Figure 11: Comparison of the PMA distribution for 'rock glacier' (blue values), 'landslide' (green values) and 'unclassifiedother' (orange values) geomorphological class vs regional topographical context (computed using average pixel frequency from TanDEM-X 12 m DEM). a) PMA mean slope; b) distribution between Top 50% average velocity PMA and PMA mean elevation; c) distribution between Top 50% average velocity and PMA surface; d) PMA slope orientation. For a) and b), the grey background represents the general slope and elevation distributionscontext of the study area, respectively.

6 Conclusions

This study developsdeveloped a robust method to detect, quantify, and analyse the surface kinematics of rock glaciers and other gravitational slopemass movements using time-series of Landsat 7/8 imagery. By integrating feature tracking fromover 24 years of imagery with time-series inversion and automatic detection of persistent moving areas (PMA), the studywe successfully monitored 153 rock glaciers and 38124229 landslides and 105 unclassified landformsgravitational mass movements over a 45x45 km² area in the semiarid Andes. The vValidation usingwith satellite radar interferometry confirmsed thethe PMA classification and their velocity attributes of the PMAs, with 42% also detected by Sentinel-1 interferograms at 12-day temporal baselines. Faster-moving landforms (2–4 m a^{-1}), primary complex ice-debris landforms, were detected. The 24-year average velocity of PMAs iswas 0.3 ± 0.07 m am yr^{-1}, with rock glaciers moving 23% faster than the median velocity of all types of geomorphological objectslandforms. Faster-moving landforms (2–4 m yr^{-1}), primary complex ice-debris landforms, were detected. Although some underestimations occurred due to the coarse pixel size, temporal data gaps and velocity field heterogeneity, decadal velocity changes were observabledetectable only for 2% of PMA dataset (n = 8). Among these PMAs, we find they have acceleration (deceleration) xas observed in 2 (1) rock glaciers, 2 landslides, and 1 (2) unclassifiedother PMAs all exceeding their respective uncertainties. under certain conditions, particularly for features exceeding 1 m a^{-1}. Below 24-year surface velocities theis threshold of threshold, tvelocity changes detected with L7/8 data were not statistically significant.ccording to our calculations, detecting decadal velocity changes below 0.4 m yr^{-1} (two times decadal NMAD values) using L7/8 data involves high uncertainty, depending on both velocity magnitude and the length of the reference period. The results of this study aligned well with existing research, and highlightinged the potential of combining radar and optical remote sensing to improve the detection and monitoring of both slow and fast gravitational mass movements. These findings enhance rock glacier mapping and kinematic understanding, particularly in the context of permafrost warming and its effectsimpact on periglacial landforms. This study demonstrates the capability of medium-resolution L7/8 imagerys for quantifying the kinematics of rock glaciers and ice-debris complex dynamics at a regional scale. It provides a methodological benchmark for assessing the state of dynamics of periglacial landforms using globally accessible, open-source optical imagery, addressing a key need within the scientific community.

Code availability. Feature tracking image correlation softwares used for this study are open-source softwares. Ames Stereo Pipeline (ASP) is available from https://stereopipeline.readthedocs.io/en/latest/introduction.html (Bayer et al., 2018) and

MicMac is available from https://micmac.ensg.eu/index.php/Accueil (Rupnick et al., 2017). Time-series inversion from optical imagery (TIO) is available from https://sourcesup.renater.fr/www/tio/. Sentinel-1 interferograms were computed using ForM@Ter LArge-scale multi-Temporal Sentinel-1 InterferoMetry processing chain (FLATSIM) based on the NSBAS pipeline. Both are available through GDM-SAR service at https://www.poleterresolide.fr/le-service-gdm-sar-in/.

Data availability. Landsat 7/8 archive freely available at http://earthexplorer.usgs.gov/. Sentinel-1 data used in our study are freely available from the ESA/EC Copernicus Sentinels Scientific Data Hub at https://scihub.copernicus.eu (Copernicus Open Access Hub, 2021). FLATSIM Sentinel-1 interferograms can be accessible upon request via Form@Ter pole (https://www.poleterresolide.fr/). TanDEM-X data are available from DLR through proposal application procedures. Data from Digital-Globe satellites (GeoEye, Ikonos, WorldView, Quickbird) and Pléiades are commercial, but programmes to facilitate academic access exist. Pleiades dataset can be accessed upon request to Ben Robson (Benjamin.Robson@uib.no). The data described in this manuscript are available at (https://zenodo.org/uploads/13119042; Cusicanqui et al., 2024) or upon request from the corresponding author (diego.cusicanqui@univ-grenoble-alpes.fr).

Supplement. The supplement related to this article is available online at: https://zenodo.org/uploads/13119042.

Author contributions. DC, PL and XB designed the study. DC performed image correlation of VHR data provided by BR and XB. PL performed image correlation of L7/8 data and implemented persistent moving area (PMA) detection. DC and PL filter GNSS dataset provided by SM and compute GNSS surface velocity time-series. DC wrote the paper with the supervision and contributions of PL. PL, XB, BR, AK and SM contributed to the discussion and edited the paper.

Competing interests. The authors declare that they have no conflict of interest.

Acknowledgment. Thanks are due to reviewers for their careful review and comments. We are grateful to the providers of free data for this study: European Space Agency (ESA)/European Commission (EC) Copernicus for Sentinel-1 data, the FLATSIM Form@TER team for their efforts processing Sentinel interferograms. Also, the German Aerospace Center (DLR) for providing the TanDEM-X DEM. We are grateful to CNES/Airbus DS for the provision of the SPOT and Pléiades satellite to the restrained dataset project 41743. We would like to thank the U.S. Geological Survey for making the Landsat 7/8 archive freely available. Thanks to GLIMS database http://glims.org/RGI/ for glacier outlines (v.6). All (or most of) the computations presented in this paper were performed using the GRICAD infrastructure (https://gricad.univ-grenoble-alpes.fr), which is supported by Grenoble research communities. Thanks to the glaciology group at CEAZA for collecting and providing the GNSS datasets, and the CHESS-funded (https://chess.w.uib.no/) "Summer school on cryospheric monitoring and water resources" for the 2022 acquisition set.

Financial support. This work has been supported by the postdoctoral program from the National Centre for Space Studies (CNES) and partially by the National Center for Scientific Research (CNRS), the program Plan d'Action pour la Prévention des Risques d'Origine Glaciaire et périglaciaire (PAPROG). This work has also been partially supported by a grant from Labex OSUG (Investissements d'avenir – ANR10 LABX56) PermANDES project. Data provided by CEAZA was supported by ANID-CENTROS REGIONALES R20F0008. Diego Cusicanqui (CNES | ISTerre), Pascal Lacroix (IRD | ISTerre), Xavier Bodin (EDYTEM | CNRS) are part of Labex OSUG (ANR10 LABX56). AK acknowledges financial support by the European Space Agency projects Permafrost_cci and EarthExplorer10 Harmony (4000123681/18/I-NB, 4000135083/21/NL/FF/ab).

References

Arenson, L., Colgan, W., and Marshall, H. P.: Chapter 2 - Physical, Thermal, and Mechanical Properties of Snow, Ice, and Permafrost, in: Snow and Ice-Related Hazards, Risks and Disasters, edited by: Shroder, J. F., Haeberli, W., and Whiteman, C., Academic Press, Boston, 35–75, https://doi.org/10.1016/B978-0-12-394849-6.00002-0, 2015.

Arenson, L. U., Harrington, J. S., Koenig, C. E. M., and Wainstein, P. A.: Mountain Permafrost Hydrology—A Practical Review Following Studies from the Andes, Geosciences, 12, 48, https://doi.org/10.3390/geosciences12020048, 2022.

Ayoub, F., Leprince, S., Binet, R., Lewis, K. W., Aharonson, O., and Avouac, J. P.: Influence of camera distortions on satellite image registration and change detection applications: 2008 IEEE International Geoscience and Remote Sensing Symposium - Proceedings, 2008 IEEE International Geoscience and Remote Sensing Symposium - Proceedings, II1072–II1075, https://doi.org/10.1109/IGARSS.2008.4779184, 2008.

Azócar, G. F. and Brenning, A.: Hydrological and geomorphological significance of rock glaciers in the dry Andes, Chile (27°-33°S): Rock Glaciers in the Dry Andes, Permafrost Periglac. Process., 21, 42–53, https://doi.org/10.1002/ppp.669, 2010.

Azócar, G. F., Brenning, A., and Bodin, X.: Permafrost distribution modelling in the semi-arid Chilean Andes, The Cryosphere, 11, 877–890, https://doi.org/10.5194/tc-11-877-2017, 2017.

Barboux, C.: Detection, mapping and monitoring of slope movements in the Alpine environment using DInSAR., PhD, University of Fribourg, 212 pp., 2014.

Berthling, I.: Beyond confusion: Rock glaciers as cryo-conditioned landforms, Geomorphology, 131, 98–106, https://doi.org/10.1016/j.geomorph.2011.05.002, 2011.

Bertone, A., Barboux, C., Bodin, X., Bolch, T., Brardinoni, F., Caduff, R., Christiansen, H. H., Darrow, M. M., Delaloye, R., Etzelmüller, B., Humlum, O., Lambiel, C., Lilleøren, K. S., Mair, V., Pellegrinon, G., Rouyet, L., Ruiz, L., and Strozzi, T.:

Incorporating InSAR kinematics into rock glacier inventories: insights from 11 regions worldwide, The Cryosphere, 16, 2769–2792, https://doi.org/10.5194/tc-16-2769-2022, 2022.

Beyer, R. A., Alexandrov, O., and McMichael, S.: The ames stereo pipeline: NASA's open source software for deriving and processing terrain data, Earth and Space Science, 5, 537–548, https://doi-org.insu.bib.cnrs.fr/10.1029/2018EA000409, 2018.

Blöthe, J. H., Halla, C., Schwalbe, E., Bottegal, E., Trombotto Liaudat, D., and Schrott, L.: Surface velocity fields of active rock glaciers and ice-debris complexes in the Central Andes of Argentina, Earth Surface Processes and Landforms, 46, 504–522, https://doi.org/10.1002/esp.5042, 2021.

Bodin, X., Thibert, E., Fabre, D., Ribolini, A., Schoeneich, P., Francou, B., Reynaud, L., and Fort, M.: Two decades of responses (1986–2006) to climate by the Laurichard rock glacier, French Alps, Permafrost Periglac. Process., 20, 331–344, https://doi.org/10.1002/ppp.665, 2009.

Bolch, T., Shea, J. M., Liu, S., Azam, F. M., Gao, Y., Gruber, S., Immerzeel, W., Kulkarni, A., Li, H., Tahir, A., Zhang, G., Zhang, Y., Bannerjee, A., Berthier, E., Brun, F., Kääb, A., Kraaijenbrink, P., Moholdt, G., Nicholson, L., Pepin, N., and Racoviteanu, A.: Status and change of the cryosphere in the Extended Hindu Kush Himalaya Region, in: The Hindu Kush Himalaya Assessment, edited by: Wester, P., Mishra, A., Mukherji, A., and Shrestha, A. B., Springer, 209–255, https://doi.org/10.1007/978-3-319-92288-1_7, 2019.

Bontemps, N., Lacroix, P., and Doin, M.-P.: Inversion of deformation fields time-series from optical images, and application to the long term kinematics of slow-moving landslides in Peru, Remote Sensing of Environment, 210, 144–158, https://doi.org/10.1016/j.rse.2018.02.023, 2018.

Brenning, A.: Spatial prediction models for landslide hazards: review, comparison and evaluation, Nat. Hazards Earth Syst. Sci., 5, 853–862, https://doi.org/10.5194/nhess-5-853-2005, 2005.

Burger, K. C., Degenhardt, J. J., and Giardino, J. R.: Engineering geomorphology of rock glaciers, Geomorphology, 31, 93–132, https://doi.org/10.1016/S0169-555X(99)00074-4, 1999.

CEAZA: Reporte anual 2012. Avalaible at www.ceazamet.cl. Accessed on Febraury 15, 2024, 2012.

CEAZA: Reporte anual 2016. Avalaible at www.ceazamet.cl. Accessed on Febraury 15, 2024, 2016.

CEAZA: Datos meteorologicos proveidos por el CEAZA. obtenidos desde. www.ceazamet.cl. Avalaible at www.ceazamet.cl. Accessed on Febraury 15, 2024, 2023.

Cicoira, A., Beutel, J., Faillettaz, J., and Vieli, A.: Water controls the seasonal rhythm of rock glacier flow, Earth and Planetary Science Letters, 528, 115844, https://doi.org/10.1016/j.epsl.2019.115844, 2019.

Cusicanqui, D., Rabatel, A., Vincent, C., Bodin, X., Thibert, E., and Francou, B.: Interpretation of Volume and Flux Changes of the Laurichard Rock Glacier Between 1952 and 2019, French Alps, Journal of Geophysical Research: Earth Surface, 126, e2021JF006161, https://doi.org/10.1029/2021JF006161, 2021.

Cusicanqui, D., Bodin, X., Duvillard, P.-A., Schoeneich, P., Revil, A., Assier, A., Berthet, J., Peyron, M., Roudnitska, S., and Rabatel, A.: Glacier, permafrost and thermokarst interactions in Alpine terrain. Insights from seven decades of reconstructed dynamics of the Chauvet glacial and periglacial system (Southern French Alps), Earth Surface Processes and Landforms, 48, 2595–2612, https://doi.org/10.1002/esp.5650, 2023.

Dehecq, A., Gourmelen, N., and Trouve, E.: Deriving large-scale glacier velocities from a complete satellite archive: Application to the Pamir–Karakoram–Himalaya, Remote Sensing of Environment, 162, 55–66, https://doi.org/10.1016/j.rse.2015.01.031, 2015.

Dehecq, A., Gardner, A. S., Alexandrov, O., McMichael, S., Hugonnet, R., Shean, D., and Marty, M.: Automated Processing of Declassified KH-9 Hexagon Satellite Images for Global Elevation Change Analysis Since the 1970s, Front. Earth Sci., 8, https://doi.org/10.3389/feart.2020.566802, 2020.

Delaloye, R., Lambiel, C., and Gärtner-Roer, I.: Overview of rock glacier kinematics research in the Swiss Alps., Geogr. Helv., 135–145, 2010.

DGA: Dinámica de Glaciares Rocosos en el Chile Semiárido: Parte I, Plan de Monitoreo., 2010.

DGA: INVENTARIO PÚBLICO DE GLACIARES, actualización 2022. SDT N°447, 2022. Ministerio de Obras Públicas, Dirección General de Aguas Unidad de Glaciología y Nieves. Realizado por: Casassa, G., Espinoza, A., Segovia, A., Huenante, J., 2022.

Doin, M.-P., Guillaso, S., Jolivet, R., Lasserre, C., Lodge, F., Ducret, G., and Grandin, R.: Presentation of the small baseline NSBAS processing chain on a case example: The Etna deformation monitoring from 2003 to 2010 using Envisat data, in: Proceedings of the Fringe symposium, Citation Key: doin2011presentation, 3434–3437, 2011.

Etzelmüller, B., Guglielmin, M., Hauck, C., Hilbich, C., Hoelzle, M., Isaksen, K., Noetzli, J., Oliva, M., and Ramos, M.: Twenty years of European mountain permafrost dynamics—the PACE legacy, Environ. Res. Lett., 15, 104070, https://doi.org/10.1088/1748-9326/abae9d, 2020.

Facciolo, G., De Franchis, C., and Meinhardt, E.: MGM: A significantly more global matching for stereovision, in: BMVC 2015, 2015.

Garreaud, R. D., Boisier, J. P., Rondanelli, R., Montecinos, A., Sepúlveda, H. H., and Veloso-Aguila, D.: The central chile mega drought (2010–2018): A climate dynamics perspective, International Journal of Climatology, 40, 421–439, https://doi.org/10.1002/joc.6219, 2020.

Gärtner-Roer, I., Brunner, N., Delaloye, R., Haeberli, W., Kääb, A., and Thee, P.: Glacier-permafrost relations in a high-mountain environment: 5 decades of kinematic monitoring at the Gruben site, Swiss Alps, The Cryosphere Discussions, 1–30, https://doi.org/10.5194/tc-2021-208, 2021.

GCOS: Plan for the Global Climate Observing System, version 1.0., 1995.

Grandin, R.: Interferometric processing of SLC sentinel-1 TOPS data, in: FRINGE'15: Advances in the science and applications of SAR interferometry and sentinel-1 InSAR workshop, frascati, italy, 23-27 march 2015, Citation Key: grandin2015interferometric, 2015.

Gruber, S.: Derivation and analysis of a high-resolution estimate of global permafrost zonation, The Cryosphere, 6, 221–233, https://doi.org/10.5194/tc-6-221-2012, 2012.

Haberkorn, A., Kenner, R., Noetzli, J., and Phillips, M.: Changes in ground temperature and dynamics in mountain permafrost in the swiss alps, Frontiers in Earth Science, 9, https://doi.org/10.3389/feart.2021.626686, 2021.

Haeberli, W. and Gruber, S.: Global warming and mountain permafrost, in: Permafrost soils, Springer, 205–218, 2009.

Haeberli, W., Hallet, B., Arenson, L., Elconin, R., Humlum, O., Kääb, A., Kaufmann, V., Ladanyi, B., Matsuoka, N., Springman, S., and Mühll, D. V.: Permafrost creep and rock glacier dynamics, Permafrost and Periglacial Processes, 17, 189–214, https://doi.org/10.1002/ppp.561, 2006.

Haeberli, W., Schaub, Y., and Huggel, C.: Increasing risks related to landslides from degrading permafrost into new lakes in de-glaciating mountain ranges, Geomorphology, 293, 405–417, https://doi.org/10.1016/j.geomorph.2016.02.009, 2017.

Halla, C., Blöthe, J. H., Tapia Baldis, C., Trombotto Liaudat, D., Hilbich, C., Hauck, C., and Schrott, L.: Ice content and interannual water storage changes of an active rock glacier in the dry Andes of Argentina, The Cryosphere, 15, 1187–1213, https://doi.org/10.5194/tc-15-1187-2021, 2021.

Hartl, L., Fischer, A., Stocker-waldhuber, M., and Abermann, J.: Recent speed-up of an alpine rock glacier: an updated chronology of the kinematics of outer hochebenkar rock glacier based on geodetic measurements, Geografiska Annaler: Series A, Physical Geography, 98, 129–141, https://doi.org/10.1111/geoa.12127, 2016.

Hartl, L., Zieher, T., Bremer, M., Stocker-Waldhuber, M., Zahs, V., Höfle, B., Klug, C., and Cicoira, A.: Multi-sensor monitoring and data integration reveal cyclical destabilization of the Äußeres Hochebenkar rock glacier, Earth Surface Dynamics, 11, 117–147, https://doi.org/10.5194/esurf-11-117-2023, 2023.

Heid, T. and Kääb, A.: Evaluation of existing image matching methods for deriving glacier surface displacements globally from optical satellite imagery, Remote Sensing of Environment, 118, 339–355, https://doi.org/10.1016/j.rse.2011.11.024, 2012.

Hock, R., Rasul, G., Adler, C., Caceres, B., Gruber, S., Hirabayashi, Y., Jackson, M., Kääb, A., Kang, S., Kutuzov, S., Milner, Al., Molau, U., Morin, S., Orlove, B., and Steltzer, H.: High Mountain Areas. In: IPCC Special Report on the Ocean and Cryosphere in a Changing Climate [H.-O. Pörtner, D.C. Roberts, V. Masson-Delmotte, P. Zhai, M. Tignor, E. Poloczanska, K. Mintenbeck, A. Alegría, M. Nicolai, A. Okem, J. Petzold, B. Rama, N.M. Weyer (eds.)]., Cambridge University Press, Cambridge, 131–202, https://doi.org/10.1017/9781009157964.004., 2019.

Höhle, J. and Höhle, M.: Accuracy assessment of digital elevation models by means of robust statistical methods, ISPRS Journal of Photogrammetry and Remote Sensing, 64, 398–406, https://doi.org/10.1016/j.isprsjprs.2009.02.003, 2009.

Hu, Y., Harrison, S., Liu, L., and Wood, J. L.: Modelling rock glacier ice content based on InSAR-derived velocity, Khumbu and Lhotse valleys, Nepal, The Cryosphere, 17, 2305–2321, https://doi.org/10.5194/tc-17-2305-2023, 2023.

Hugonnet, R., McNabb, R., Berthier, E., Menounos, B., Nuth, C., Girod, L., Farinotti, D., Huss, M., Dussaillant, I., Brun, F., and Kääb, A.: Accelerated global glacier mass loss in the early twenty-first century, Nature, 592, 726–731, https://doi.org/10.1038/s41586-021-03436-z, 2021.

IANIGLA: Inventario Nacional de Glaciares 2018. Resumen ejecutivo de los resultados del Inventario Nacional de Glaciares. IANIGLA-CONICET, Ministerio de Ambiente y Desarrollo Sustentable de la Nacion. Pp. 27, 2018.

Janke, J. and Frauenfelder, R.: The relationship between rock glacier and contributing area parameters in the Front Range of Colorado, Journal of Quaternary Science, 23, 153–163, https://doi.org/10.1002/jqs.1133, 2008.

Janke, J., Bellisario, A., and Ferrando, F.: Classification of debris-covered glaciers and rock glaciers in the Andes of central Chile, Geomorphology, 241, https://doi.org/10.1016/j.geomorph.2015.03.034, 2015.

Jansen, F. and Hergarten, S.: Rock glacier dynamics: Stick-slip motion coupled to hydrology, Geophysical Research Letters, 33, https://doi.org/10.1029/2006GL026134, 2006.

Kääb, A., Frauenfelder, R., and Roer, I.: On the response of rockglacier creep to surface temperature increase, Global and Planetary Change, 56, 172–187, https://doi.org/10.1016/j.gloplacha.2006.07.005, 2007.

Kääb, A., Strozzi, T., Bolch, T., Caduff, R., Trefall, H., Stoffel, M., and Kokarev, A.: Inventory and changes of rock glacier creep speeds in Ile Alatau and Kungöy Ala-Too, northern Tien Shan, since the 1950s, The Cryosphere, 15, 927–949, https://doi.org/10.5194/tc-15-927-2021, 2021.

Kääb, A. and Røste, J.: Rock glaciers across the United States predominantly accelerate coincident with rise in air temperatures, Nat Commun, 15, 7581, https://doi.org/10.1038/s41467-024-52093-z, 2024.

Kalthoff, N., Bischoff-Gauß, I., Fiebig-Wittmaack, M., Fiedler, F., Thürauf, J., Novoa, E., Pizarro, C., Castillo, R., Gallardo, L., Rondanelli, R., and Kohler, M.: Mesoscale Wind Regimes in Chile at 30°S, Journal of Applied Meteorology and Climatology, 41, 953–970, https://doi.org/10.1175/1520-0450(2002)041<0953:MWRICA>2.0.CO;2, 2002.

Kaufmann, V., Kellerer-Pirklbauer, A., and Seier, G.: Conventional and UAV-Based Aerial Surveys for Long-Term Monitoring (1954–2020) of a Highly Active Rock Glacier in Austria, Frontiers in Remote Sensing, 2, 2021.

Kellerer-Pirklbauer, A. and Kaufmann, V.: About the relationship between rock glacier velocity and climate parameters in central Austria, Austrian Journal of Earth Sciences, 105, 94–112, 2012.

Kellerer-Pirklbauer, A., Lieb, G. K., and Kaufmann, V.: Rock Glaciers in the Austrian Alps: A General Overview with a Special Focus on Dösen Rock Glacier, Hohe Tauern Range, in: Landscapes and Landforms of Austria, edited by: Embleton-Hamann, C., Springer International Publishing, Cham, 393–406, https://doi.org/10.1007/978-3-030-92815-5_27, 2022.

Kellerer-Pirklbauer, A., Bodin, X., Delaloye, R., Lambiel, C., Gärtner-Roer, I., Bonnefoy-Demongeot, M., Carturan, L., Damm, B., Eulenstein, J., Fischer, A., Hartl, L., Ikeda, A., Kaufmann, V., Krainer, K., Matsuoka, N., Cella, U. M. D., Noetzli, J., Seppi, R., Scapozza, C., Schoeneich, P., Stocker-Waldhuber, M., Thibert, E., and Zumiani, M.: Acceleration and interannual variability of creep rates in mountain permafrost landforms (rock glacier velocities) in the European Alps in 1995–2022, Environmental Research Letters, 19, 034022, https://doi.org/10.1088/1748-9326/ad25a4, 2024.

Kenner, R., Phillips, M., Beutel, J., Hiller, M., Limpach, P., Pointner, E., and Volken, M.: Factors Controlling Velocity Variations at Short-Term, Seasonal and Multiyear Time Scales, Ritigraben Rock Glacier, Western Swiss Alps, Permafrost and Periglac. Process., 28, 675–684, https://doi.org/10.1002/ppp.1953, 2017.

Kenner, R., Pruessner, L., Beutel, J., Limpach, P., and Phillips, M.: Why rock glacier deformation velocities correlate with both ground temperatures and water supply at multiple temporal scales, , https://doi.org/10.5194/egusphere-egu2020-9534, 2020.

Kooistra, L., Berger, K., Brede, B., Graf, L. V., Aasen, H., Roujean, J.-L., Machwitz, M., Schlerf, M., Atzberger, C., Prikaziuk, E., Ganeva, D., Tomelleri, E., Croft, H., Reyes Muñoz, P., Garcia Millan, V., Darvishzadeh, R., Koren, G., Herrmann, I., Rozenstein, O., Belda, S., Rautiainen, M., Rune Karlsen, S., Figueira Silva, C., Cerasoli, S., Pierre, J., Tanır Kayıkçı, E., Halabuk, A., Tunc Gormus, E., Fluit, F., Cai, Z., Kycko, M., Udelhoven, T., and Verrelst, J.: Reviews and syntheses: Remotely sensed optical time series for monitoring vegetation productivity, Biogeosciences, 21, 473–511, https://doi.org/10.5194/bg-21-473-2024, 2024.

Kunz, J. and Kneisel, C.: Glacier–Permafrost Interaction at a Thrust Moraine Complex in the Glacier Forefield Muragl, Swiss Alps, Geosciences, 10, 205, https://doi.org/10.3390/geosciences10060205, 2020.

Lacroix, P., Araujo, G., Hollingsworth, J., and Taipe, E.: Self-Entrainment Motion of a Slow-Moving Landslide Inferred From Landsat-8 Time Series, Journal of Geophysical Research: Earth Surface, 124, 1201–1216, https://doi.org/10.1029/2018JF004920, 2019.

Lacroix, P., Dehecq, A., and Taipe, E.: Irrigation-triggered landslides in a Peruvian desert caused by modern intensive farming, Nat. Geosci., 13, 56–60, https://doi.org/10.1038/s41561-019-0500-x, 2020a.

Lacroix, P., Handwerger, A. L., and Bièvre, G.: Life and death of slow-moving landslides, Nat Rev Earth Environ, 1, 404–419, https://doi.org/10.1038/s43017-020-0072-8, 2020b.

Lacroix, P., Belart, J. M. C., Berthier, E., Sæmundsson, Þ., and Jónsdóttir, K.: Mechanisms of Landslide Destabilization Induced by Glacier-Retreat on Tungnakvíslarjökull Area, Iceland, Geophysical Research Letters, 49, e2022GL098302, https://doi.org/10.1029/2022GL098302, 2022.

Lehmann, B., Anderson, R. S., Bodin, X., Cusicanqui, D., Valla, P. G., and Carcaillet, J.: Alpine rock glacier activity over Holocene to modern timescales (western French Alps), Earth Surface Dynamics Discussions, 1–40, https://doi.org/10.5194/esurf-2022-8, 2022.

Leprince, S., Berthier, E., Ayoub, F., Delacourt, C., and Avouac, J.-P.: Monitoring Earth Surface Dynamics With Optical Imagery, Eos, Transactions American Geophysical Union, 89, 1–2, https://doi.org/10.1029/2008EO010001, 2008.

MacDonell, S., Farías, P. N., Aliste, V., Ayala, Á., Guzmán, C., Díaz, P. J., Schaffer, N., Schauwecker, S., Sproles, E. A., and Francisco, E. Y. S.: Snow and ice in the desert: reflections from a decade of connecting cryospheric science with communities in the semiarid Chilean Andes, Annals of Glaciology, 63, 158–164, https://doi.org/10.1017/aog.2023.51, 2022.

Magnin, F., Ravanel, L., Bodin, X., Deline, P., Malet, E., Krysiecki, J.-M., and Schoeneich, P.: Main results of permafrost monitoring in the French Alps through the PermaFrance network over the period 2010–2022, Permafrost and Periglacial Processes, 35, 3–23, https://doi.org/10.1002/ppp.2209, 2024.

Manchado, A. M.-T., Allen, S., Cicoira, A., Wiesmann, S., Haller, R., and Stoffel, M.: 100 years of monitoring in the Swiss National Park reveals overall decreasing rock glacier velocities, Commun Earth Environ, 5, 1–17, https://doi.org/10.1038/s43247-024-01302-0, 2024.

Marcer, M., Cicoira, A., Cusicanqui, D., Bodin, X., Echelard, T., Obregon, R., and Schoeneich, P.: Rock glaciers throughout the French Alps accelerated and destabilised since 1990 as air temperatures increased, Commun Earth Environ, 2, 1–11, https://doi.org/10.1038/s43247-021-00150-6, 2021.

Markham, B. L., Storey, J. C., Williams, D. L., and Irons, J. R.: Landsat sensor performance: history and current status, IEEE Transactions on Geoscience and Remote Sensing, 42, 2691–2694, https://doi.org/10.1109/TGRS.2004.840720, 2004.

Masiokas, M. H., Villalba, R., Luckman, B. H., Quesne, C. L., and Aravena, J. C.: Snowpack Variations in the Central Andes of Argentina and Chile, 1951–2005: Large-Scale Atmospheric Influences and Implications for Water Resources in the Region, Journal of Climate, 19, 6334–6352, https://doi.org/10.1175/JCLI3969.1, 2006.

Masiokas, M. H., Villalba, R., Luckman, B. H., and Mauget, S.: Intra- to Multidecadal Variations of Snowpack and Streamflow Records in the Andes of Chile and Argentina between 30° and 37°S, Journal of Hydrometeorology, 11, 822–831, https://doi.org/10.1175/2010JHM1191.1, 2010.

Monnier, S. and Kinnard, C.: Reconsidering the glacier to rock glacier transformation problem: New insights from the central Andes of Chile, Geomorphology, 238, 47–55, https://doi.org/10.1016/j.geomorph.2015.02.025, 2015.

Monnier, S. and Kinnard, C.: Interrogating the time and processes of development of the Las Liebres rock glacier, central Chilean Andes, using a numerical flow model, Earth Surface Processes and Landforms, 41, 1884–1893, https://doi.org/10.1002/esp.3956, 2016.

Monnier, S. and Kinnard, C.: Internal structure and composition of a rock glacier in the Andes (upper Choapa valley, Chile) using borehole information and ground-penetrating radar, Annals of Glaciology, 54, 61–72, https://doi.org/10.3189/2013AoG64A107, 2013.

Monnier, S., Kinnard, C., Surazakov, A., and Bossy, W.: Geomorphology, internal structure, and successive development of a glacier foreland in the semiarid Chilean Andes (Cerro Tapado, upper Elqui Valley, 30 08′ S., 69 55′ W.), Geomorphology, 207, 126–140, 2014.

Montecinos, A. and Aceituno, P.: Seasonality of the ENSO-Related rainfall variability in central chile and associated circulation anomalies, Journal of Climate, 16, 281–296, https://doi.org/10.1175/1520-0442(2003)016<0281:SOTERR>2.0.CO;2, 2003.

Müller, J., Vieli, A., and Gärtner-Roer, I.: Rockglaciers on the run - Understanding rockglacier landform evolution and recent changes from numerical flow modeling, The Cryosphere Discussions, 1–40, https://doi.org/10.5194/tc-2016-35, 2016.

Navarro, G., MacDonell, S., and Valois, R.: A conceptual hydrological model of semiarid Andean headwater systems in Chile, Progress in Physical Geography: Earth and Environment, 47, 668–686, https://doi.org/10.1177/03091333221147649, 2023a.

Navarro, G., Valois, R., MacDonell, S., de Pasquale, G., and Díaz, J. P.: Internal structure and water routing of an ice-debris landform assemblage using multiple geophysical methods in the semiarid Andes, Frontiers in Earth Science, 11, https://doi.org/10.3389/feart.2023.1102620, 2023b.

Noetzli, J., Biskaborn, B. K., Christiansen, H. H., Isaksen, K., Schoeneich, P., Smith, P., Vieira, G., Zhao, L., and Streletskiy, D. A.: Permafrost thermal state. In Bull. Amer. Meteor. Soc. Vol. 100., in: State of Climate 2018, vol. 9, Bull. Amer. Meteor. Soc., 21–22, 2019.

Notarnicola, C.: Hotspots of snow cover changes in global mountain regions over 2000–2018, Remote Sensing of Environment, 243, 111781, https://doi.org/10.1016/j.rse.2020.111781, 2020.

Nuth, C. and Kääb, A.: Co-registration and bias corrections of satellite elevation data sets for quantifying glacier thickness change, The Cryosphere, 5, 271–290, https://doi.org/10.5194/tc-5-271-2011, 2011.

Obu, J.: How Much of the Earth's Surface is Underlain by Permafrost?, Journal of Geophysical Research: Earth Surface, 126, e2021JF006123, https://doi.org/10.1029/2021JF006123, 2021.

de Pasquale, G., Valois, R., Schaffer, N., and MacDonell, S.: Contrasting geophysical signatures of a relict and an intact Andean rock glacier, The Cryosphere, 16, 1579–1596, https://doi.org/10.5194/tc-16-1579-2022, 2022.

Patton, A. I., Rathburn, S. L., and Capps, D. M.: Landslide response to climate change in permafrost regions, Geomorphology, 340, 116–128, https://doi.org/10.1016/j.geomorph.2019.04.029, 2019.

Pei, Y., Qiu, H., Yang, D., Liu, Z., Ma, S., Li, J., Cao, M., and Wufuer, W.: Increasing landslide activity in the Taxkorgan River Basin (eastern Pamirs Plateau, China) driven by climate change, CATENA, 223, 106911, https://doi.org/10.1016/j.catena.2023.106911, 2023.

Pellet, C., Bodin, X., Cusicanqui, D., Delaloye, R., Kaab, A., Kaufmann, V., Noetzli, J., Thibert, E., Vivero, S., and Kellerer-Pirklbauer, A.: Rock glacier velocity, Bull. Amer. Meteor. Soc., 103, Si-S465, https://doi.org/10.1175/2022BAMSStateoftheClimate.1, 2022.

Poblete, A. G. and Minetti, J. L.: ¿Influye el calentamiento global en la disminución de las nevadas en los Andes Áridos?, Revista Universitaria de Geografía, 26, 11–29, 2017.

Réveillet, M., MacDonell, S., Gascoin, S., Kinnard, C., Lhermitte, S., and Schaffer, N.: Impact of forcing on sublimation simulations for a high mountain catchment in the semiarid Andes, The Cryosphere, 14, 147–163, https://doi.org/10.5194/tc-14-147-2020, 2020.

RGI Consortium: Randolph Glacier Inventory – A Dataset of Global Glacier Outlines: Version 6.0: Technical Report, Global Land Ice Measurements from Space., https://doi.org/10.7265/N5-RGI-60, 2017.

RGIK: Guidelines for inventorying rock glaciers, https://doi.org/10.51363/unifr.srr.2023.002, 2023.

Robson, B. A., MacDonell, S., Ayala, Á., Bolch, T., Nielsen, P. R., and Vivero, S.: Glacier and rock glacier changes since the 1950s in the La Laguna catchment, Chile, The Cryosphere, 16, 647–665, https://doi.org/10.5194/tc-16-647-2022, 2022.

Rosu, A.-M., Pierrot-Deseilligny, M., Delorme, A., Binet, R., and Klinger, Y.: Measurement of ground displacement from optical satellite image correlation using the free open-source software MicMac, ISPRS Journal of Photogrammetry and Remote Sensing, 100, 48–59, https://doi.org/10.1016/j.isprsjprs.2014.03.002, 2015.

Rupnik, E., Daakir, M., and Pierrot Deseilligny, M.: MicMac – a free, open-source solution for photogrammetry, Open Geospatial Data, Software and Standards, 2, 14, https://doi.org/10.1186/s40965-017-0027-2, 2017.

Schaffer, N. and MacDonell, S.: Brief communication: A framework to classify glaciers for water resource evaluation and management in the Southern Andes, The Cryosphere, 16, 1779–1791, https://doi.org/10.5194/tc-16-1779-2022, 2022.

Schaffer, N., MacDonell, S., Réveillet, M., Yáñez, E., and Valois, R.: Rock glaciers as a water resource in a changing climate in the semiarid Chilean Andes, Reg Environ Change, 19, 1263–1279, https://doi.org/10.1007/s10113-018-01459-3, 2019.

Schauwecker, S., Palma, G., MacDonell, S., Ayala, Á., and Viale, M.: The Snowline and 0°C Isotherm Altitudes During Precipitation Events in the Dry Subtropical Chilean Andes as Seen by Citizen Science, Surface Stations, and ERA5 Reanalysis Data, Front. Earth Sci., 10, https://doi.org/10.3389/feart.2022.875795, 2022.

Scherler, D., Leprince, S., and Strecker, M. R.: Glacier-surface velocities in alpine terrain from optical satellite imagery—Accuracy improvement and quality assessment, Remote Sensing of Environment, 112, 3806–3819, https://doi.org/10.1016/j.rse.2008.05.018, 2008.

Smith, M. J.: Chapter Eight - Digital Mapping: Visualisation, Interpretation and Quantification of Landforms, in: Developments in Earth Surface Processes, vol. 15, edited by: Smith, M. J., Paron, P., and Griffiths, J. S., Elsevier, 225–251, https://doi.org/10.1016/B978-0-444-53446-0.00008-2, 2011.

Sorg, A., Kääb, A., Roesch, A., Bigler, C., and Stoffel, M.: Contrasting responses of Central Asian rock glaciers to global warming, Scientific Reports, 5, 8228, https://doi.org/10.1038/srep08228, 2015.

Stammler, M., Cusicanqui, D., Bell, R., Robson, B., Bodin, X., Blöthe, J., and Schrott, L.: Vertical surface change signals of rock glaciers: combining UAV and Pléiades imagery (Agua Negra, Argentina), https://doi.org/10.52381/ICOP2024.138.1, 2024.

Strozzi, T., Caduff, R., Jones, N., Barboux, C., Delaloye, R., Bodin, X., Kääb, A., Mätzler, E., and Schrott, L.: Monitoring Rock Glacier Kinematics with Satellite Synthetic Aperture Radar, Remote Sensing, 12, 559, https://doi.org/10.3390/rs12030559, 2020.

Stumpf, A., Malet, J.-P., and Delacourt, C.: Correlation of satellite image time-series for the detection and monitoring of slow-moving landslides, Remote Sensing of Environment, 189, 40–55, https://doi.org/10.1016/j.rse.2016.11.007, 2017.

Sun, Z., Hu, Y., Racoviteanu, A., Liu, L., Harrison, S., Wang, X., Cai, J., Guo, X., He, Y., and Yuan, H.: TPRoGI: a comprehensive rock glacier inventory for the Tibetan Plateau using deep learning, Earth System Science Data Discussions, 1–32, https://doi.org/10.5194/essd-2024-28, 2024.

Thibert, E. and Bodin, X.: Changes in surface velocities over four decades on the Laurichard rock glacier (French Alps), Permafrost and Periglacial Processes, 33, 323–335, https://doi.org/10.1002/ppp.2159, 2022.

Thollard, F., Clesse, D., Doin, M.-P., Donadieu, J., Durand, P., Grandin, R., Lasserre, C., Laurent, C., Deschamps-Ostanciaux, E., Pathier, E., Pointal, E., Proy, C., and Specht, B.: FLATSIM: The ForM@Ter LArge-Scale Multi-Temporal Sentinel-1 InterferoMetry Service, Remote Sensing, 13, 3734, https://doi.org/10.3390/rs13183734, 2021.

Toth, C. and Jóźków, G.: Remote sensing platforms and sensors: A survey, ISPRS Journal of Photogrammetry and Remote Sensing, 115, 22–36, https://doi.org/10.1016/j.isprsjprs.2015.10.004, 2016.

Trombotto, D., Buk, E., and Hernández, J.: Rock glaciers in the southern central Andes (approx. 33–34 S), Cordillera Frontal, Mendoza, Argentina, Bamberger Geographische Schriften, 19, 145–173, 1999.

Ustin, S. L. and Middleton, E. M.: Current and near-term advances in Earth observation for ecological applications, Ecological Processes, 10, 1, https://doi.org/10.1186/s13717-020-00255-4, 2021.

Villarroel, C., Tamburini Beliveau, G., Forte, A., Monserrat, O., Morvillo, M., Villarroel, C. D., Tamburini Beliveau, G., Forte, A. P., Monserrat, O., and Morvillo, M.: DInSAR for a Regional Inventory of Active Rock Glaciers in the Dry Andes Mountains of Argentina and Chile with Sentinel-1 Data, Remote Sensing, 10, 1588, https://doi.org/10.3390/rs10101588, 2018.

Vivero, S., Bodin, X., Farías-Barahona, D., MacDonell, S., Schaffer, N., Robson, B. A., and Lambiel, C.: Combination of aerial, satellite, and UAV photogrammetry for quantifying rock glacier kinematics in the dry andes of chile (30°S) since the 1950s, Frontiers in Remote Sensing, 2, https://doi.org/10.3389/frsen.2021.784015, 2021.

Wagner, T., Kainz, S., Krainer, K., and Winkler, G.: Storage-discharge characteristics of an active rock glacier catchment in the Innere Ölgrube, Austrian Alps, Hydrological Processes, 35, e14210, https://doi.org/10.1002/hyp.14210, 2021.

Wirz, V., Geertsema, M., Gruber, S., and Purves, R. S.: Temporal variability of diverse mountain permafrost slope movements derived from multi-year daily GPS data, Mattertal, Switzerland, Landslides, 13, 67–83, https://doi.org/10.1007/s10346-014-0544-3, 2016.

Wood, E., Bolch, T., and Streeter, R.: Insights from feature tracking of optical satellite data for studying rock glacier kinematics in the Northern Tien Shan, Front. Earth Sci., 12, https://doi.org/10.3389/feart.2024.1518390, 2025.

Hu, Y., et al. (15 co-authors). Rock Glacier Velocity as a new product of the Essential Climate Variable Permafrost. Fernández, J., Bonsoms, J., García-Oteyza, J., & Oliva, M. (Eds.) (2023): 6th European Conference on Permafrost – Book of Abstracts, 18 June – 22 June 2023, Puigcerdà, 308. https://doi.org/10.52381/EUCOP6.abstracts.1, 2023